

Journal of Geophysical Research: Solid Earth

RESEARCH ARTICLE

10.1002/2013JB010802

Key Points:

- Demagnetization of the shallow and deep substratum occurs in hydrothermal areas
- We develop methods for mapping and modeling concealed hydrothermal alteration
- Alteration is confined into narrow structures reaching depth of a few 100 m

Correspondence to:

C. Bouligand,
Claire.Bouligand@ujf-grenoble.fr

Citation:

Bouligand, C., J. M. G. Glen, and R. J. Blakely (2014), Distribution of buried hydrothermal alteration deduced from high-resolution magnetic surveys in Yellowstone National Park, *J. Geophys. Res. Solid Earth*, 119, 2595–2630, doi:10.1002/2013JB010802.

Received 30 OCT 2013

Accepted 4 MAR 2014

Accepted article online 11 MAR 2014

Published online 7 APR 2014

Distribution of buried hydrothermal alteration deduced from high-resolution magnetic surveys in Yellowstone National Park

Claire Bouligand^{1,2}, Jonathan M.G. Glen³, and Richard J. Blakely³

¹University Grenoble Alpes, ISTerre, Grenoble, France, ²CNRS, ISTerre, Grenoble, France, ³U.S. Geological Survey, Menlo Park, California, USA

Abstract Yellowstone National Park (YNP) displays numerous and extensive hydrothermal features. Although hydrothermal alteration in YNP has been extensively studied, the volume, geometry, and type of rock alteration at depth remain poorly constrained. In this study, we use high-resolution airborne and ground magnetic surveys and measurements of remanent and induced magnetization of field and drill core samples to provide constraints on the geometry of hydrothermal alteration within the subsurface of three thermal areas in YNP (Firehole River, Smoke Jumper Hot Springs, and Norris Geyser Basin). We observe that hydrothermal zones from both liquid- and vapor-dominated systems coincide with magnetic lows observed in aeromagnetic surveys and with a decrease of the amplitude of short-wavelength anomalies seen in ground magnetic surveys. This suggests a strong demagnetization of both the shallow and deep substratum within these areas associated with the removal of magnetic minerals by hydrothermal alteration processes. Such demagnetization is confirmed by measurements of rock samples from hydrothermal areas which display significantly decreased total magnetization. A pronounced negative anomaly is observed over the Lone Star Geyser and suggests a significant demagnetization of the substratum associated with areas displaying large-scale fluid flow. The ground and airborne magnetic surveys are used to evaluate the distribution of magnetization in the subsurface. This study shows that significant demagnetization occurs over a thickness of at least a few hundred meters in hydrothermal areas at YNP and that the maximum degree or maximum thickness of demagnetization correlates closely with the location of hydrothermal activity and mapped alteration.

1. Introduction

Yellowstone National Park (YNP) is a volcanic province shaped by three cycles of caldera formation (at ~2.1 Ma, ~1.3 Ma, and ~0.64 Ma) associated with the deposition of ash flow tuffs and subsequent rhyolite and basalt flows [Christiansen, 2001]. YNP also displays numerous well-developed and complex hydrothermal systems distributed mainly within or along the 0.6 Ma caldera rim (Figure 1) that differ in water chemistry, occurrence and composition of hydrothermal deposits, and nature of hydrothermal alteration reactions [Fournier, 1989]. These characteristics depend on the nature and permeability of the surrounding rocks but also on the geographic location of the outflow (above or near the water table) and are believed to have evolved over time (e.g., as a consequence of the change in the water table level, as observed during the transition from the last glaciation; White *et al.* [1971]). Two main types of hydrothermal systems are generally distinguished in YNP, although several systems are more complex and share characteristics of both types of systems [e.g., White, 1957; Fournier, 1989; Lowenstein *et al.*, 2012]. In liquid-dominated systems, hot waters flowing from subsurface high-temperature reservoirs tend to dissolve the rock. Waters issuing from these systems are neutral to basic, Cl⁻ and SiO₂ rich, occur at low elevation, and deposit amorphous silica. In vapor-dominated systems, steam rises from deep boiling hydrothermal reservoirs. Waters issuing from these systems occur at high elevation and represent mixtures of perched groundwater and condensed steam. They are typically acid and SO₄²⁻ rich and tend to transform the superficial substratum to clay. In this paper, the different processes that lead to a change of rock chemistry and mineralogy after interactions with hydrothermal fluids will be referred to as "hydrothermal alteration". Such processes include both the dissolution and modification of rocks by deep hot waters and the acid alteration of superficial substrata by condensed steams. Although hydrothermal systems in the Park have

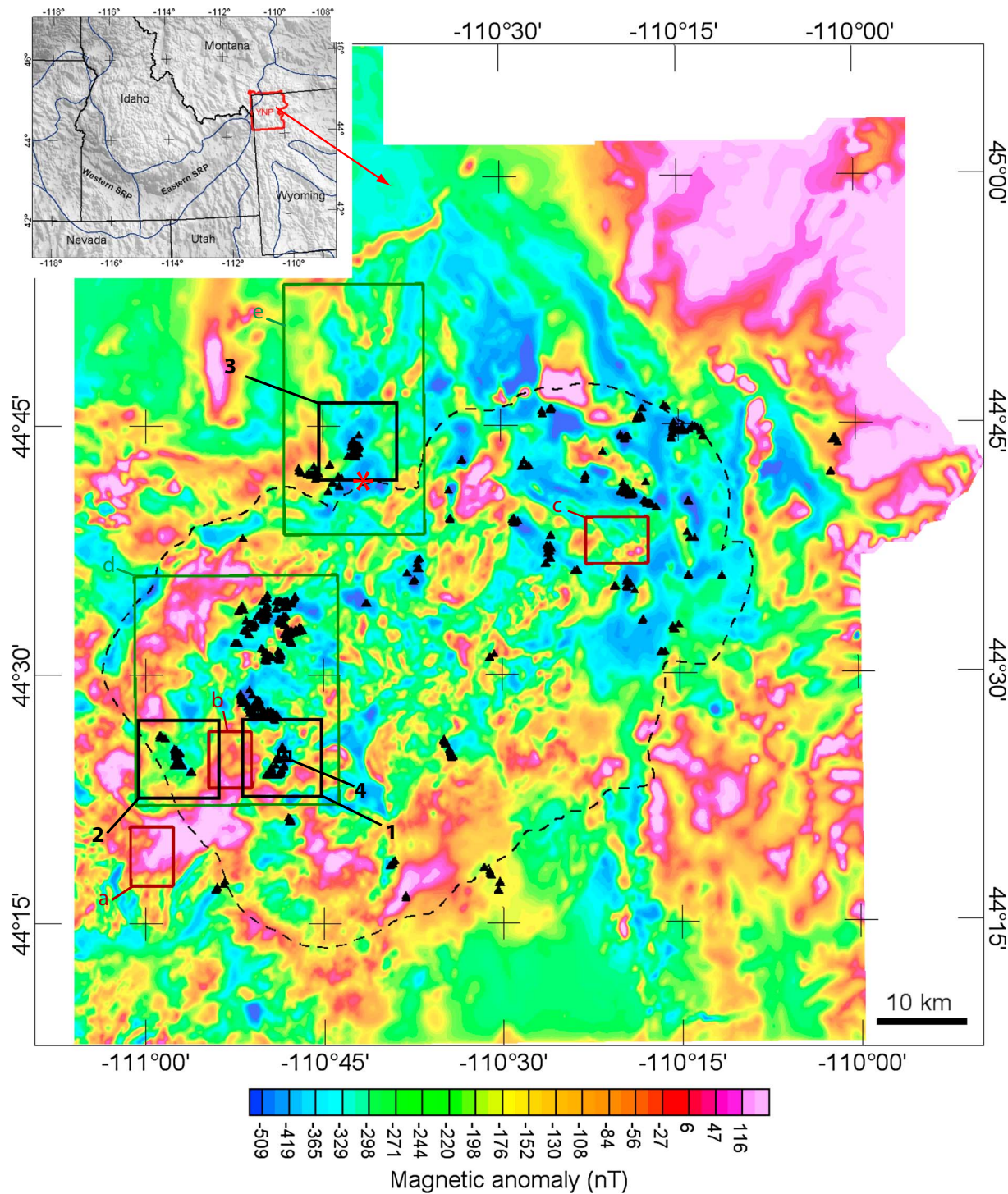


Figure 1. Map of the high-resolution aeromagnetic survey of Yellowstone National Park. Aeromagnetic anomalies are reduced to the pole. Thermal features are located by black triangles. The dashed outline represents the 0.6 Ma Caldera rim [after Christiansen, 2001]. Note that magnetic lows are generally associated with thermal features. Black rectangles show the location of study areas, whereas brown rectangles show the location of areas selected to estimate magnetization of unaltered substratum. Green rectangles show the location of larger areas described in the discussion and presented in Figures 17 and 18. The red star shows the center of a negative anomaly associated with contacts between rock units and discussed in the text. (top left) Index map showing the location of YNP.

been extensively studied through field observations [e.g., Christiansen and Wahl, 1999; Christiansen, 2001], remote-sensing imagery [e.g., Hellman and Ramsey, 2004; Livo et al., 2007], water chemistry [e.g., Fournier, 1989], and core drilling [e.g., White et al., 1975], the volume and geometry of hydrothermal alteration in the subsurface remain poorly constrained.

Magnetic surveys can help to map and evaluate the extent of hydrothermal alteration, as demonstrated by Finn and Morgan [2002] with a high-resolution aeromagnetic survey of Yellowstone National Park [U. S. Geological Survey, 2000]. Indeed, this work revealed that, after reduction to the pole of the aeromagnetic map (Figure 1), areas of hydrothermal activity generally display magnetic lows. Most areas of hydrothermal activity in YNP are localized within substrata that were formed during or after the formation of the 0.6 Ma caldera and thus entirely within the Brunhes normal epoch that began ~0.78 Ma. Therefore, the substratum hosts normal polarity magnetization, and magnetic anomaly lows imply a decrease in magnetization. This suggests that hydrothermal alteration of the substratum and of its magnetic minerals has led to a significant decrease in magnetization [Finn and Morgan, 2002]. Many of these magnetic lows extend beyond the limits of surface alteration and hot springs, indicating that larger extents of altered rock may lie at depth. Finn and Morgan [2002] proposed preliminary estimates of the distribution of hydrothermal alteration in the subsurface of two hydrothermal areas in YNP by constructing 2-D models of the crustal magnetization that account for the observed magnetic lows and by assuming that hydrothermal alteration has completely destroyed the rock magnetization. In the following, the decrease or loss of the substratum magnetization in areas of hydrothermal activity is referred to as demagnetization. This demagnetization could be due to two different processes: removal or transformation of the substratum magnetic minerals by hydrothermal alteration as suggested by Finn and Morgan [2002] or to thermal demagnetization of the substratum in areas where its temperature is above the Curie temperature (~580°C). However, extrapolation of temperature measurements performed in drill holes within the park suggests that the substratum temperature is not higher than 310°C at a depth of 1 km [White et al., 1975] indicating that demagnetization of the shallow substratum cannot be explained by thermal demagnetization.

Hydrothermal alteration in YNP transforms magnetite into weakly magnetic minerals such as hematite, goethite, montmorillonite, and pyrite [e.g., Bargar and Muffler, 1982; Bargar and Beeson, 1984; White et al., 1988]. However, the effects of hydrothermal alteration on magnetic mineralogy and on substratum magnetization properties are not expected to be the same in liquid-dominated systems, where the environment is usually reducing, and vapor-dominated systems, where the environment is usually oxidizing. Hochstein and Soengkono [1997] suggested that magnetite may be more stable in vapor-dominated systems because of its oxidizing environment but also that acidic condensates formed near the surface in these vapor-dominated systems can dissolve magnetite.

The first purpose of this study is to test if hydrothermal alteration in YNP leads to a significant decrease of the substratum magnetization, as assumed by Finn and Morgan [2002], if this demagnetization is complete or partial, if it is observed in different types of hydrothermal systems existing in YNP, and if hydrothermal alteration of the substratum can explain the magnetic lows observed in the aeromagnetic map. The second purpose of this study is to develop and test methods using high-resolution magnetic surveys to perform detailed mapping of alteration and to evaluate the geometry of subsurface alteration. To this end, we focused on four study areas in YNP displaying both hydrothermal alteration and magnetic lows. In these study areas, we investigated the magnetic properties of fresh and hydrothermally altered geologic units by compiling existing and new rock sample measurements of magnetic susceptibility and remanence intensity and direction. Although the aeromagnetic survey available in YNP is of relatively high resolution, we acquired new ground-based magnetic surveys to provide a more detailed mapping of magnetic anomalies in the selected study areas. Ground magnetic profiles were used to evaluate the amplitude of short-wavelength anomalies and the depth to magnetic sources in order to test if demagnetization of the shallow volcanic substratum occurs in hydrothermal areas. Magnetic grids constructed from airborne and ground-based data were used to invert the distribution of magnetization, relying on various simplifying assumptions and taking the topography into account. These models were used to infer the distribution of hydrothermal alteration. In the following sections, we present the selected study areas, the characteristics of ground-based and airborne surveys used in this study, a compilation of magnetic measurements performed on rock samples from the study areas, results of computations and inversions based on the ground and airborne data, and finally, a discussion of results.

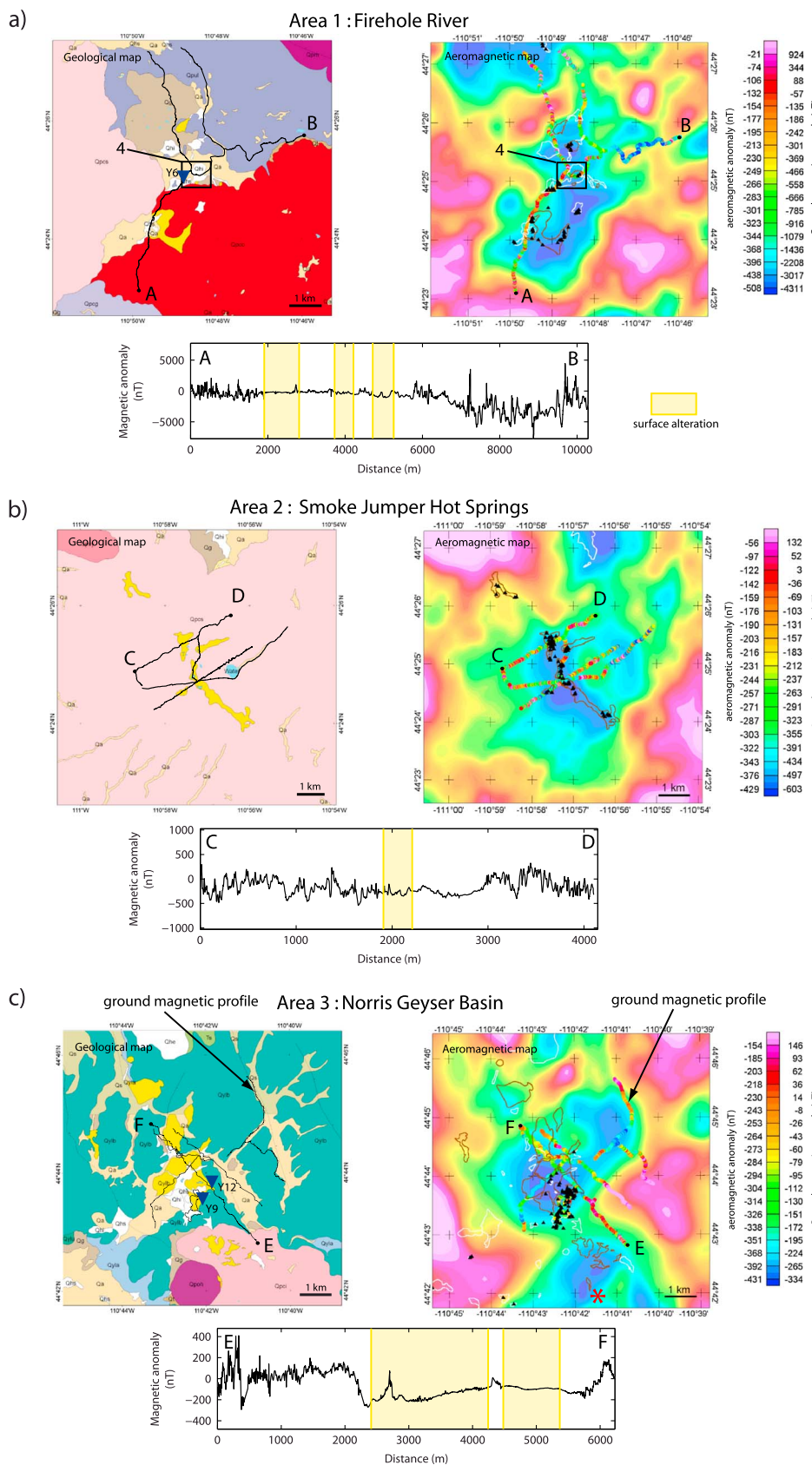


Figure 2

d) **Legend****Location of data**

- magnetic profile
- drill hole from 67-68

Hydrothermal features

- hydrothermal deposits
- hydrothermal alteration
- thermal spring

Geology

- water
- Qa - Aluvium and glacio-fluvial deposits
- Qg - Glacial deposits

Lava Creek Tuff

- Qylb - Member B
- Qyla - Member A
- Qylu - Upper part of Member A

Plateau Rhyolite*Central Plateau Members*

- Qpcg - Grants Pass flow
- Qpcy - West Yellowstone flow
- Qpcs - Summit Lake flow
- Qpcc - Spring Creek flow
- Qpci - Gibbon River flow

Mallard Lake Members

- Qpm - Mallard Lake flow
- Qpoh - Gibbon Hill Dome

Upper Basin Members

- Qpul - Scaup Lake flow

Figure 2. (continued)**2. Study Areas**

We selected four study areas displaying magnetic lows associated with hydrothermal activity and alteration (Figures 1 and 2): area 1 along Firehole River, area 2 around Smoke Jumper Hot Springs, area 3 in Norris Geyser Basin, and area 4 (which is a subarea of area 1) around Lone Star Geyser. These hydrothermal areas have different characteristics in terms of topography, nature of surrounding rocks, hydrothermal water chemistry, occurrence and composition of hydrothermal deposits, and nature of hydrothermal alteration reactions.

The Firehole River area (Figures 1 and 2a) is located inside the 0.6 Ma caldera rim, in the valley, and at the border of three rhyolite flows: the Spring Creek, Summit Lake, and Scaup Lake flows. Its hydrothermal manifestations include Lone Star Geyser but also many hot springs with rather low discharge. Because the water table is only a few meters below ground [see *White et al.*, 1975], this area is a liquid-dominated system with thermal fluids that are principally neutral to basic and rich in Cl^- and SiO_2 , typical of liquid-dominated systems. Some acid SO_4^{2-} rich waters, produced by steam condensation, are also observed over topographic highs in this area. Analysis of drill core Y-6 (Firehole River, Figure 2a) shows that alteration is principally located along fractures and cavities [*Bargar and Beeson*, 1984]. Thermal waters have deposited siliceous sinter such as the Lone Star Geyser cone.

The Smoke Jumper Hot Springs area (Figures 1 and 2b) is located near the inferred 0.6 Ma caldera rim, on a rhyolite plateau composed of the Summit Lake flow. It displays mostly fumaroles and low-discharge hot springs. Because the water table is a few hundred meters below ground, Smoke Jumper Hot Springs is a vapor-dominated system. Its thermal fluids represent mixtures of perched groundwater and condensed steam and are acid and SO_4^{2-} rich, which is typical of vapor-dominated systems [e.g., *White*, 1957; *Lowenstern et al.*, 2012]. No drill cores were taken in this area, and no hydrothermal deposits are present at the surface, but information about hydrothermal alteration can be inferred from drill core Y-11 (Mud Volcano) located within a relatively similar vapor-dominated system. This drill core shows at least two stages of alteration [*Bargar and Muffler*, 1982] suggesting that the Mud Volcano geothermal system and

possibly also the Smoke Jumper Hot Springs area evolved from a liquid-dominated system (with near-neutral Cl^- rich SO_4^{2-} poor fluids that deposited silica) to a vapor-dominated system (with acid and SO_4^{2-} rich fluids and clay alteration) most likely by a drop in the hydrostatic head of the liquid-dominated system during postglacial times.

The Norris Geyser Basin area (Figures 1 and 2c), which displays numerous geysers and hot springs, is located outside the 0.6 Ma caldera rim. Its substratum is composed of the relatively impermeable Lava Creek Tuff, confining water circulation along fractures. Because the water table is only a few meters below the surface, this area is a liquid-dominated system. *White et al.* [1988] gave a detailed description of its thermal fluids,

hydrothermal alteration, and deposits. Thermal fluids display a large variety in chemistry with neutral to acid waters, various contents in Cl^- , SiO_2 , and SO_4^{2-} , and various degree of dilution with meteoritic waters. Drill cores Y-9 (Norris Basin I), Y-12 (Norris Basin II), and C-II (Carnegie II) show that the Lava Creek Tuff was affected by at least three stages of alteration: an early pervasive oxidizing stage that mobilized and deposited iron oxides such as magnetite, hematite, and goethite and stained the tuffs, a reducing stage affecting nearby fractures or permeable zones that transformed iron oxides into sulfides such as pyrite and bleached the tuffs, and finally, a superficial acid alteration stage that bleached the tuffs white. Such different stages indicate several episodes of sealing and reopening of the geothermal system with subsequent changes in the thermal water chemistry. In addition, hydrothermal hot springs and geysers deposited amorphous silica in the form of siliceous cemented sediment and sinter.

Substrata exposed in the study areas are composed of rhyolite flows or ash flow tuffs that were formed during or after the formation of the 0.6 Ma caldera and thus entirely within the Brunhes normal epoch that began ~0.78 Ma. We expect, therefore, that the study areas are underlain by substrata hosting a normal polarity magnetization. The Lava Creek Tuff that was deposited during formation of the last caldera has an estimated thickness of ~300–400 m in the Firehole River and Lone Star Geyser areas, ~0–50 m in the Smoke Jumper area, and ~350–400 m in the Norris Geyser area [see Christiansen, 2001]. These tuffs are overlain by a thick rhyolite plateau in the Smoke Jumper Hot Springs, Firehole River, and Lone Star Geyser areas, with a maximum thickness of ~300 m. Therefore, the substrata in our study areas host a normal polarity over at least a thickness of several hundred meters.

3. Magnetic Surveys

3.1. High-Resolution Aeromagnetic Survey

The high-resolution aeromagnetic survey conducted over YNP in 1997 [U. S. Geological Survey, 2000] offers a unique opportunity to study the buried extent of relatively shallow features such as hydrothermal alteration across a large area including regions difficult to access. This total field magnetic survey was collected along east-west flight lines spaced 400 m and included a few north-south tie lines to facilitate leveling of the flight line data. The survey was draped at about 250 m above the terrain with flight elevation recorded with both barometric and radar altimeters. Magnetic measurements were corrected for the strength of the main field predicted using the International Geomagnetic Reference Field (IGRF), leveled to correct for small discrepancies between flight-line and tie-line data, gridded with a 100 m spacing, and decorrugated to remove noise resulting from very small baseline shifts between adjacent flight lines [U. S. Geological Survey, 2000]. The projection used to construct this grid and also used in all maps presented in this paper (except the index map shown in Figure 1) is UTM12N with the WGS84 datum. In order to help interpretation of magnetic anomalies, we also reduced the aeromagnetic grid to the pole, using the standard phase filter [e.g., Blakely, 1995] and assuming a constant inclination $I = 70^\circ$ and declination $D = 14^\circ$ for both the regional magnetic field and the substratum magnetization (valid for induced magnetization, recent volcanic terrain, or rocks with remanence dominated by an expected normal overprint). The effect of this correction is a slight shift of anomaly extrema toward their causative source. Note that the reduction to the pole filter used here assumes that the survey is recorded at a constant elevation, which is not the case. Some small distortions may arise because of this assumption. However, all models of magnetization intensity discussed subsequently were derived from original magnetic anomaly grids not reduced to the pole.

Figure 2. Geologic map, aeromagnetic map, and one ground magnetic profile for study areas 1–3: (a) Firehole river, (b) Smoke Jumper Hot Springs, and (c) Norris Geyser Basin. The geological map and unit names are from the digital geological map of YNP [National Park Service, 2007] built from Christiansen and Blank [1974] and Christiansen [1975]. Aeromagnetic maps are not reduced to the pole for consistency with the ground data. Ground magnetic profiles are represented by black lines on the geologic maps and colored circles on the aeromagnetic maps. Yellow polygons (on the geological maps) and brown outlines (on the aeromagnetic maps) are areas of acid hydrothermal alteration. White polygons (on the geological maps) and white outlines (on the aeromagnetic maps) are areas of hydrothermal deposits including hot spring deposits (Qh , Qhs , and Qhc), ice-contact deposits localized by hot springs (Qhi), and hydrothermal explosion deposits (Qhe) from National Park Service [2007]. Endpoints of displayed magnetic profiles are indicated by letters (AB, CD, or EF). The distance scale is obtained by adding distance between successive measurement points. Extent of surface alteration (deduced from the geologic map) along these profiles is represented in yellow. Location of study area 4 (Lone Star Geyser) is indicated by a black square. The red star shows the center of a negative anomaly associated with contacts between rock units and discussed in the text. (d) Legend for geologic maps.

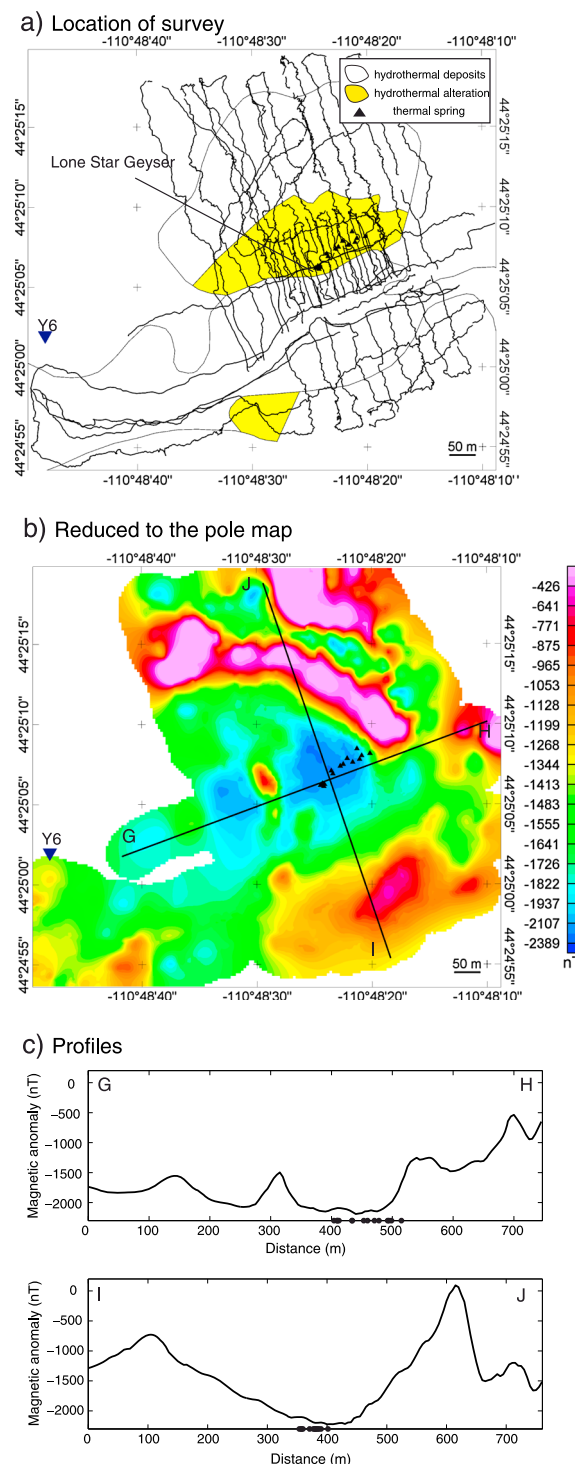


Figure 3. Location of (a) ground magnetic survey, (b) magnetic anomaly map, and (c) profiles in study area 4 (Lone Star Geyser). Magnetic anomalies have been reduced to the pole based on a magnetic field direction of $I = 70^\circ$, $D = 14^\circ$. Location of ground magnetic profiles is indicated by black thick lines in Figure 3a. Areas of acid hydrothermal alteration and hydrothermal deposits [after Christiansen and Blank, 1974] are represented in Figure 3a by yellow and white polygons (with a thin black outline), respectively. Thermal features are represented by black triangles. Figure 3c shows cross sections of the reduced to the pole grid (Figure 3b) taken along the black lines labeled GH and IJ. Black dots in Figure 3c are projected positions of hydrothermal features.

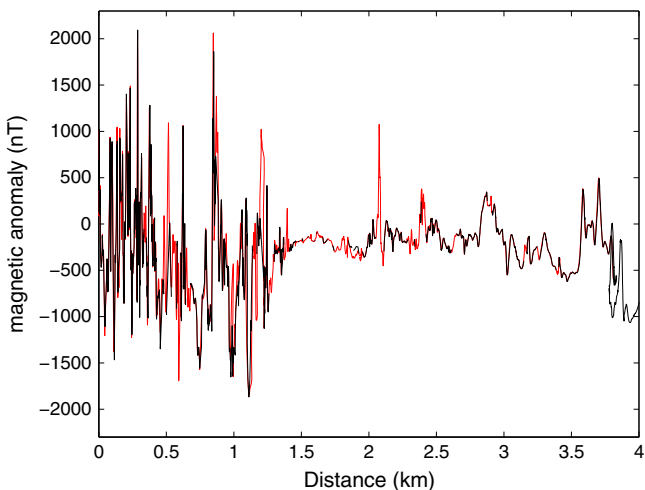


Figure 4. Subset of profile AB (corresponding to its first 5 km) from area 1 (Firehole River) shown in Figure 2a measured in the A to B (black) and B to A (red) directions. The distance scale is obtained after projecting the coordinates of the profile along a direction of azimuth +45° and is different from the distance scale used in Figure 2. Note that profiles are very similar. There is no significant horizontal or vertical shift of measured anomalies. Discontinuities in the black profile correspond to positions where no measurements were available (due to “drop outs” in the magnetic recording).

area 3 (Norris Geyser Basin) and centered over the Gibbon River flow (Qpci) and Gibbon Hill dome (Qpoh) which are adjacent to the Lava Creek Tuff (Qyl) to the north and to other rhyolite flows, the Nez Perce Creek (Qpcn) and the Solfatara Plateau (Qpof) flows to the south. This negative anomaly indicates that the Qpci and Qpoh units have a much lower magnetization than adjacent units. As mentioned earlier, the aeromagnetic map also displays magnetic lows centered on areas of hydrothermal activity and surface alteration. Figure 2 shows subsets of the aeromagnetic map in areas 1–3 that contain such magnetic lows. *Finn and Morgan [2002]* suggest that the lows result from a significant decrease of the substratum magnetization caused by hydrothermal alteration. Note that hydrothermal alteration and deposits are also visible on the Qpci and Qpoh units mentioned above. Therefore, the lower magnetization of these units could be due to a more intense alteration of these units in comparison to adjacent units.

3.2. Ground Magnetic Surveys

In order to better understand the relationship between magnetic lows and hydrothermal alteration, we performed, during the fall of 2008 and 2010, ground-based magnetic surveys using a cesium vapor magnetometer at ~2 m above ground. These surveys include several 4–5 km long transects acquired with a 1 s sample rate while walking at a normal pace (~1.3 m sample interval) across thermal features within study areas 1–3 (Firehole River, Smoke Jumper Hot Springs, and Norris Geyser Basin; Figure 2), and a detailed survey over an area of about 800 m × 500 m acquired with a 0.1 s sample rate (~0.13 m sample interval) around Lone Star Geyser (Figure 3). The detailed survey was conducted along approximately north-northwest oriented lines with a line spacing of about 10 m (near thermal features) to 50 m (far from thermal features) and with a few transverse tie lines. Diurnal magnetic field variations were recorded using a proton precession base station magnetometer which remained at a fixed location. We corrected magnetic anomaly profiles for diurnal variations even though these variations never exceeded 50 nT, far less than the variations measured along profiles, of a few 100 nT to a few 1000 nT. Some of the ground profiles were repeated to check for consistency. We observed that the short- and long-wavelength signals are very well reproduced (Figure 4).

Figure 2 displays the location of magnetic transects in study areas 1–3 and a sample profile for each. Ground magnetic transects acquired over unaltered volcanic terrain generally display large-amplitude short-wavelength anomalies due to the existence of significant contrasts of magnetization in the shallow

The aeromagnetic map (Figure 1) displays many short- and long-wavelength anomalies that are due to contrasts of magnetization associated either with topography (contrast of magnetization intensity between the bedrock and the air), with contacts between different rock types or units, or with chemical transformations such as hydrothermal alteration that modify rock magnetic properties. Magnetic anomalies associated with topography are obvious in the northeast corner of the YNP survey, over the Absaroka Mountains, where positive anomalies are correlated with topographic highs (Figure 1). An example of a magnetic anomaly associated with contacts between rock units is the negative anomaly located by a red star (see Figures 1 and 2c) on the southern border of

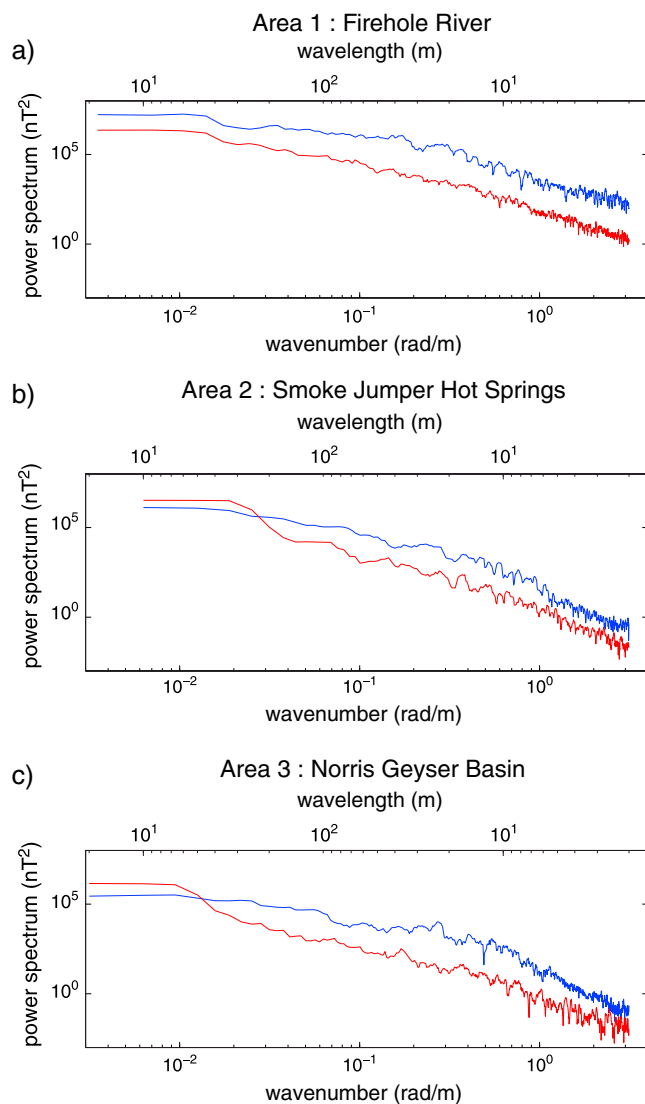


Figure 5. Power spectra of magnetic anomalies computed using the multitaper method (described in *Percival and Walden [1993]*) from (a) profile AB in area 1 (Firehole River), (b) profile CD in area 2 (Smoke Jumper Hot Springs), and (c) profile EF in area 3 (Norris Geyser Basin). Spectra in red are for portions of profile over inferred altered areas and in blue over inferred unaltered areas. Distances used along profile AB are 0 m to 1800 m (unaltered) and 2000 m to 3800 m (altered), along profile CD are 0 m to 1000 m (unaltered) and 2000 m to 3000 m (altered), and along EF are 0 m to 2000 m (unaltered) and 3000 m to 5000 m (altered).

substratum (e.g., resulting from local changes in the chemistry and mineralogy of the flow). Although characterized by different amplitudes, this short-wavelength signal is observed over all three study areas (anomaly amplitudes of a few 100 nT over the Lava Creek Tuff in Norris Geyser Basin and of 500–1000 nT over the rhyolite flows in the Firehole River and the Smoke Jumper Hot Springs areas). On the other hand, the short-wavelength anomaly signal is of very low amplitude in hydrothermally altered areas indicating the absence of or very low magnetization of shallow sources. In fact, power spectra of magnetic anomaly profiles over altered and unaltered areas (Figure 5) show that the amplitude of signals with wavelengths shorter than about 200–300 m (i.e., wave numbers larger than about 2×10^{-2} to 3×10^{-2} rad/m) is decreased by a factor of at least 10 within altered areas. This contrast in the magnetic signal between unaltered and altered substratum strongly suggests pervasive and nearly complete demagnetization of the shallow volcanic basement by hydrothermal alteration. Note that for areas 1 and 3, some segments of the magnetic transect cross a layer of alluvium that covers the volcanic substratum. Although derived from the nearby volcanic substratum, such a layer of alluvium may have low to negligible magnetization because it is composed of

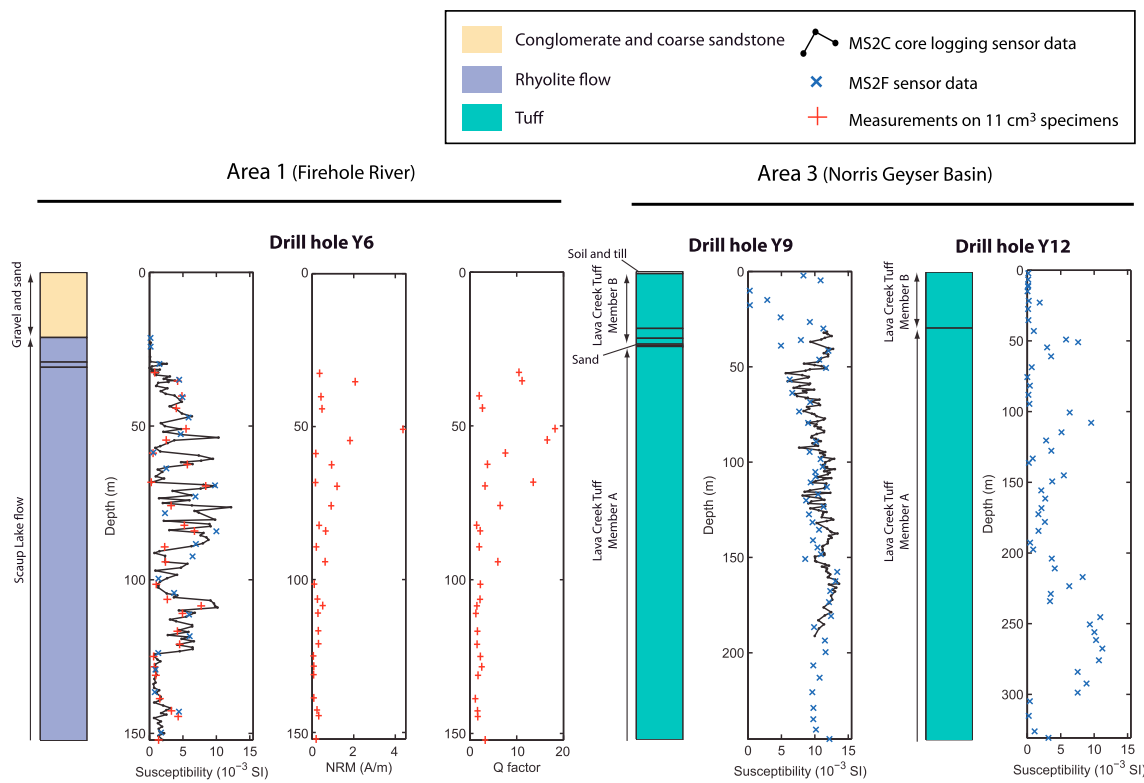


Figure 6. Lithology and magnetic properties of drill cores Y6 (Firehole River), Y9 (Norris Basin I), and Y12 (Norris Basin II). Black dots and blue crosses are susceptibility measurements made using a Bartington MS2C core logging sensor and a Bartington MS2F surface point probe, respectively. Red plus signs are measurements of susceptibility, natural remanent magnetization (NRM), and Koenigsberger (Q) ratio made on 11 cm³ specimens using a Bartington MS2B sensor and a 2G cryogenic magnetometer. MS2F data were obtained after averaging four readings made on the surface of the core and applying a calibration factor of 4.4 estimated from the ratio of averaged values measured with MS2C sensor and averaged values measured with MS2F probe.

randomly oriented and likely weathered and weakly magnetic material. Therefore, alluvium may also contribute to the damping of magnetic anomalies (Figure 2). A pronounced relatively large-wavelength magnetic low coincides with the zone of suppressed anomalies in Norris Geyser Basin (see profile EF, Figure 2c), whereas only subdued magnetic lows are observed in the Smoke Jumper Hot Springs and Firehole River areas (see profiles AB and CD, Figures 2a and 2b). This could be due to a deeper extent of magnetization, a stronger contrast of magnetization intensity between altered and unaltered units, or a different geometry of the altered body at Norris Geyser Basin.

Figure 3a displays the location of survey lines acquired in area 4 (Lone Star Geyser). Measurement locations were determined with the magnetometer's built-in GPS which has an accuracy of ~1 m at best, but with significantly lower accuracy over forested areas. For this reason, GPS data were first despiked and smoothed with a 100 data point moving window. Despite this cleaning, a certain amount of noise remains in the location data as observed in Figure 3a. Magnetic data discrepancies at line intersections are, however, relatively small (averaged value of 14.7 nT and standard deviation of 33.5 nT) compared to magnetic anomaly amplitudes observed over the survey area (~500–1000 nT) and were therefore not corrected. Magnetic data were then gridded with a 5 m spacing using a minimum curvature algorithm and reduced to the pole using the same direction for the regional magnetic field and the substratum magnetization ($I = 70^\circ$, $D = 14^\circ$; Figure 3b). Cross sections of this magnetic grid are represented in Figure 3c in order to better evaluate the width and amplitude of the magnetic low observed in the center of the survey area.

Although located within an area characterized by damped ground magnetic anomalies (see profile AB of Figure 2), this detailed survey displays several prominent magnetic anomalies (Figures 3b and 3c), indicating that rocks from this area, although less magnetic than unaltered volcanic terrain, are not completely nonmagnetic. Reduction to the pole tends to slightly shift anomalies northward. As a result the pronounced

Table 1. Volume Susceptibility χ , Intensity J_{NRM} , Declination D , and Inclination I of Natural Remanent Magnetization (NRM), 95% Confidence Cone α_{95} , Koenigsberger (Q) Ratio, and Number of Samples for Rhyolite Flows (Scaup Lake Flow and Summit Lake Flow) and Lava Creek Tuff Compiled From the Literature and Measured on Samples From Drill Cores and Collected in the Field^a

χ (10 ⁻³ SI)	J_{NRM} (A/m)	D (deg)	I (deg)	α_{95} (deg)	Q factor	No. Samples	Source
<i>Lava Creek Tuff (Qyl)</i>							
4.9 (4.3–5.8)		1.8 (344.2–15.9)	65.9 (54.2–76.5)	2.1		5 157	Oliver and Christiansen [1998] Reynolds [1977]
0.60	5.94	4.9	64.6		21.3	NS	Finn and Morgan [2002]
10.8 (5.6–13.6)						162	MS2C data from Y12
9.5 (0.25–13.4)						51	MS2F data from Y9
3.6 (0.033–11.2)						54	MS2F data from Y12
0.51 (0.004–2.3)	0.16 (0.0008–0.49)			25.2 (1.03–47.4)		5	11 cm ³ cores from field samples
<i>Summit Lake Flow (Qpc)</i>							
0.17 (0.004–0.53)	0.57 (0.0008–2.26)			73.6 (4.38–144.9)		14	11 cm ³ cores from field samples
<i>Scaulp Lake Flow (Qpu)</i>							
0.64	2.9	4	55.6	9.1		NS	Finn and Morgan [2002]
3.4 (0.27–8.4)	0.63 (0.060–4.4)		58.1 (46.9–72.2)	4.7 (1.2–18.2)		28	11 cm ³ cores from Y6
3.3 (0.04–12.2)						160	MS2C data from Y6
3.9 (0.14–10.0)						24	MS2F data from Y6
<i>Lava Creek Tuff and Post 0.6 Myr-Caldera Rhyolite Flows</i>							
(0.12–5.9)	(0.21–1.45)	356.9	61.9	4.8	(0.67–23.8)	46 sites	Harlan and Morgan [2008]

^aFor each type of measurement, average value and range of measured values (given in parentheses) are provided when available. NS means “not specified”. Inclination and declination are for the NRM except for data from Reynolds [1977] which are characteristic remanent directions estimated after alternating field (AF) demagnetization. Q ratios were computed assuming a magnetic field strength of 44 A/m (except for data from Finn and Morgan [2002] who assumed a field strength of 44.6 A/m and Harlan and Morgan [2008] whose assumption is not specified). The last line of the table displays summarized results from Harlan and Morgan [2008] including samples from both rhyolite flows and the Lava Creek Tuff.

magnetic low with approximate amplitude of 500 nT and diameter of 130 m in the center of the survey becomes more closely centered on the Lone Star Geyser and associated hot springs, suggesting that the low is caused by demagnetization directly associated with the hydrothermal plumbing system feeding the Geyser and nearby springs. Another prominent feature of this magnetic survey is a 50 m wide elongated positive anomaly located just north of the magnetic low and the hot springs. This anomaly is not correlated with topography, surface geology, or hydrothermal features. It may be caused by a lava flow concealed below the detrital deposits (Qa), which is ~25 m thick in drill core Y6 (Figure 6), as the anomaly width is similar to the detrital layer thickness.

4. Rock Properties

Because of the nonuniqueness of potential field problems, it is not possible to unequivocally determine the 3-D distribution of magnetization in the subsurface from measurements of the magnetic field. In order to reduce the number of unknowns in the problem, we constrain the magnetic properties of geologic units available in our study areas by compiling in Table 1 measurements of the magnetic susceptibility χ and of the natural remanent magnetization (NRM) intensity and direction available in the literature [Reynolds, 1977; Oliver and Christiansen, 1998; Finn and Morgan, 2002; Harlan and Morgan, 2008] and new measurements performed on samples collected in the study areas and from drill cores (cores Y6: Firehole River, Y9: Norris Basin I, and Y12: Norris Basin II). When possible, we provide both an averaged value and the range of observed values obtained over a set of samples from the same unit. The Koenigsberger (Q) ratio is the ratio of the intensities of remanent magnetization J_{NRM} and induced magnetization:

$$Q = \frac{J_{\text{NRM}}}{\chi H} \quad \text{and} \quad H = \frac{B}{\mu_0}$$

where H is the magnetic field strength, B is the magnetic induction, and $\mu_0 = 4\pi \cdot 10^{-7} \text{ Hm}^{-1}$ is the magnetic permeability of free space. Between the aeromagnetic survey flown in the fall of 1997 and the ground detailed magnetic survey collected in the fall of 2010, the intensity B of the main geomagnetic field predicted by IGRF models [Finlay et al., 2010] in YNP decreased from ~55,800 nT to ~54,500 nT corresponding to a decrease in H from ~44.4 A/m to ~43.4 A/m. We therefore assumed a mean value for H

of ~ 44 A/m for the computation of Q ratios. Note that averaged Q ratios are different from ratios of averaged values for remanent and induced magnetization. When available, we also provide the 95% confidence cone, α_{95} , to quantify uncertainty on the averaged NRM directions. Inclinations and declinations provided by Reynolds [1977] for the Lava Creek Tuff are not NRM directions but best fit mean directions of the characteristic remanent directions estimated after applying stepwise alternating field (AF) demagnetization. However, the author mentions that differences between NRM and characteristic remanent directions are small ($< 10^\circ$).

We performed new remanence and susceptibility measurements samples using a 2G cryogenic magnetometer and a Bartington susceptibility meter with a MS2B sensor on 11 cm^3 specimens drilled from unoriented hand samples (as we did not have National Park Service authorization to drill paleomagnetic samples) collected in the field and from drill core. Additional susceptibility measurements were collected from whole drill core samples using a Bartington susceptibility meter first with a MS2F surface point probe in contact with the samples (for cores Y6, Y9, and Y12) and second passing the samples through a MS2C core logging sensor (for cores Y6 and Y9). MS2F and MS2C readings can differ. Indeed, the MS2F probe is sensitive to material within a 2 cm^2 area and 90% of the signal comes from within the uppermost 6 mm under the surface. On the other hand, the MS2C sensor is sensitive to material up to one coil diameter (8 cm) away from the sensor with 70% of the signal coming from material up to a quarter of the coil diameter away. For these reasons, the MS2F sensor provides susceptibility values that are dependent on the mineralogy immediately below the probe, whereas the MS2C sensor provides an estimation of the whole-rock susceptibility. To overcome this difficulty, four measurements (two on the sides and two on the ends of core segments) were taken with the MS2F probe and averaged for each core sample. Moreover, as the MS2F is not buried in the sample but placed against its surface, the reading could provide at most 50% of the rock susceptibility or an even smaller percentage as the contact between the probe and the rugged surface of the sample was not perfect. Despite these pitfalls, we observed a clear correlation between MS2C and MS2F data but with lower readings provided by the MS2F probe. We estimated a ratio of 4.4 between averaged readings obtained using MS2C and MS2F sensors and applied this factor to the MS2F readings (see Figure 6). Other examples of cross calibration between a MS2F probes and other susceptibility meters are discussed in Lecoanet *et al.* [1999]. Although less accurate, the MS2F data are of particular interest because they provide information on the susceptibility of the topmost part of drill core Y9 whose diameter was too large to pass through the MS2C sensor and for drill core Y12 which was not measured with the MS2C sensor because of time limitations.

Table 1 shows a large range of values for magnetic susceptibility and NRM intensity that we interpret as reflecting different degrees of weathering or hydrothermal alteration. Assessing effects of hydrothermal alteration on the magnetic properties of rock units requires being able to compare magnetic properties of fresh and hydrothermally altered samples. We assume that the magnetic properties published in the literature [Finn and Morgan, 2002; Oliver and Christiansen, 1998; Reynolds, 1977] were obtained from samples that are either unaltered or affected by a relatively low degree of alteration and thus can be used to constrain the properties of fresh units. In contrast, our new measurements were performed on samples taken from outcrops and drill core located within or close to mapped hydrothermal sites. Most of these samples show evidence of hydrothermal alteration and/or weathering. Although it may be difficult to distinguish hydrothermal alteration from weathering, we consider the drill core measurements to reflect the properties of hydrothermally altered units, assuming the flows were subject to minimal exposure prior to the deposition of subsequent units.

Published measurements performed on samples from the Lava Creek Tuff (Qyl), which constitute most of the substratum of the Norris Geyser Basin area, show average values for magnetic susceptibility of $\sim 0.6 \times 10^{-3}$ to 5×10^{-3} SI, NRM intensity of ~ 6 A/m, and Q ratio of ~ 20 indicating that remanent magnetization is dominant in the fresh (i.e., unaltered) tuffs. Among the three main rhyolite flows composing the substratum of the Smoke Jumper Hot Springs and the Firehole River areas, we have no published measurements available for the Spring Creek Flow (Qpcc) and the Summit Lake Flow (Qpcs). We therefore assume that the magnetic properties of the Scaup Lake Flow (Qpul) evaluated on paleomagnetic samples from Finn and Morgan [2002] are representative of fresh rhyolite flows present over our study areas. These measurements indicate average susceptibility values of $\sim 0.6 \times 10^{-3}$ SI, NRM intensity of ~ 3 A/m, and Q ratio of ~ 9 , indicating that remanent magnetization is also dominant in the fresh rhyolite flows.

Rhyolite and tuff samples collected from drill cores and outcrops located in or nearby hydrothermal sites show a large variability of NRM intensities and magnetic susceptibility, with values ranging over at least 2 orders of magnitude and with maximum values similar to those of fresh samples. The remanent magnetization remains nevertheless dominant in these samples (Q ratios larger than 1 except within a few samples where it is close to 1). Such variability suggests that the degree of hydrothermal alteration is highly variable within hydrothermal areas. In order to better understand the effect of hydrothermal alteration on magnetic susceptibility and NRM intensity, we address the variation of these parameters as a function of depth in drill cores Y6 (Firehole River), Y9 (Norris Basin I), and Y12 (Norris Basin II) (Figure 6).

Magnetic susceptibilities, NRM intensities, and Q factors measured in drill core Y6, located in the center of Firehole River hydrothermal area (Figure 2), show large variations (with minimum and maximum values spanning more than a factor of 10) probably due to different degrees of hydrothermal alteration of the Scaup Lake Flow. Inspection of hydrothermal minerals present in drill core Y6 shows a large range of iron-rich minerals characterized by low magnetic susceptibility and remanence such as hematite, goethite, and pyrite [Bargar and Beeson, 1984] indicating that hydrothermal alteration transformed the iron oxides initially present in the rhyolite flows into less magnetic minerals. This suggests that hydrothermal alteration of rhyolite flows in the Firehole River area leads to a significant decrease of the total magnetization. The varying magnetic susceptibility and remanence within the drill core indicate that this alteration and its subsequent demagnetization are not homogenously distributed.

Magnetic susceptibilities measured in drill cores Y9 and Y12, both located at the margin of the Norris Geyser Basin hydrothermal area (see location in Figure 2), show very different patterns. Drill core Y9 displays very small variations and large values of magnetic susceptibility (around 10×10^{-3} SI) except at the topmost part of the drill core where very small values of the magnetic susceptibility are observed. On the other hand, drill core Y12 shows relatively large variations but principally small values of magnetic susceptibility with almost null magnetic susceptibility at the topmost part of the core. Although both Y9 and Y12 show clear indications of hydrothermal alteration of the Lava Creek Tuff (e.g., groundmass stained to yellow or red) throughout most of the drill cores, White *et al.* [1988] indicated that among the three stages of hydrothermal alteration observed in drill core Y12, only two of them were observed in drill core Y9. The first stage of alteration was pervasive and affected both cores. It deposited iron oxides, such as magnetite, hematite, and goethite, and stained the tuff. As magnetic susceptibilities are fairly high in drill core Y9, we conclude that this stage of alteration did not decrease the tuff magnetization, but instead, may have contributed to the total magnetization of the tuffs due to the deposition of magnetite. The second stage of alteration was limited to fractures or permeable zones and was observed only in core Y12. This stage transformed iron oxides into minerals characterized by low magnetic susceptibility and zero remanence (pyrite, montmorillonite, other clays and chlorite) and bleached the tuff white. Note that periods of iron oxide deposition are locally superimposed on this bleaching second stage in core Y12 indicating changes in fluid composition. The much lower magnetic susceptibilities observed in Y12 compared to Y9 suggest that the second stage significantly decreased the magnetic susceptibility of the tuff. The heterogeneous distribution of this alteration and the local deposition of new iron oxides likely account for the variability of magnetic susceptibility values. Finally, the third stage of alteration also bleached the tuff white, deposited sulfides such as pyrite (and locally some pyrrhotite, characterized by larger magnetic susceptibility and remanence [e.g., Hunt *et al.*, 1995]), was limited to the near surface, and was observed in both drill cores. This last stage may explain the significant decrease of magnetic susceptibility near the surface. Although we do not have measurements of the NRM intensity in drill cores Y9 and Y12, we assume it mimics the decrease in magnetic susceptibility since the fine-grained titanomagnetite carrying the stable magnetization [Reynolds, 1977] likely also dominates the susceptibility. The comparison of the nearby drill cores Y9 and Y12 shows that hydrothermal alteration and subsequent demagnetization can vary significantly over short distances, probably because alteration is highly dependent on fluid permeability.

Although we do not have access to magnetic properties and magnetic mineralogy of the substratum beneath the Smoke Jumper Hot Springs area, we may infer information from drill core Y-11 (Mud Volcano) located within a relatively similar vapor-dominated system but in ash flow tuffs instead of a rhyolite flow for the Smoke Jumper Hot Springs area. Assemblages of hydrothermal alteration minerals observed in drill core Y-11 indicate the existence of two stages of alteration [Bargar and Muffler, 1982]. The early stage deposited

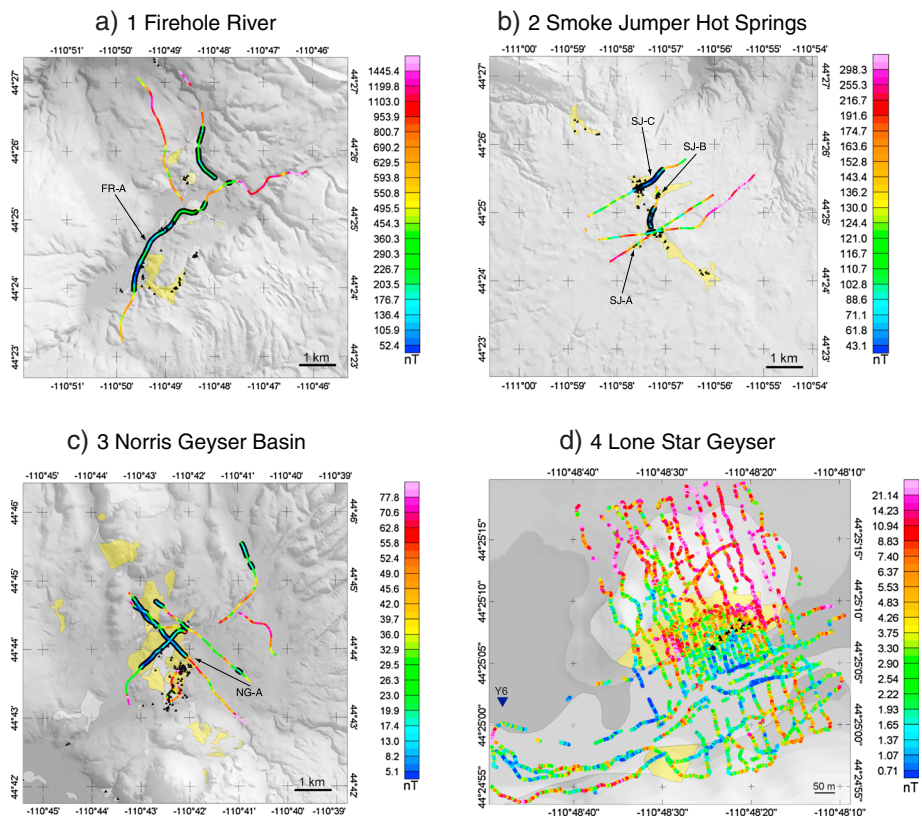


Figure 7. Standard deviation of magnetic anomalies computed over regularly spaced overlapping windows in study areas 1–4. (a) Firehole River, (b) Smoke Jumper Hot Springs, (c) Norris Geyser Basin, and (d) Lone Star Geyser. The window width is 500 m in areas 1–3 (Figures 7a–7c) and 10 m in area 4 (Figure 7d). Adjacent windows overlap over 90% of their length. In areas 1–3, symbols are underlain by a black thick line in zones of inferred hydrothermal alteration based on the value of the standard deviation being lower than a given threshold (<330 nT for area 1, <75 nT for area 2, and <20 nT for area 3). Areas of acid hydrothermal alteration and hydrothermal deposits are indicated by yellow and white polygons, respectively. Thermal features are represented by black triangles. These symbols are represented over shaded topography in the background. Note that the color scale is different for each area.

minerals typical of water-dominated systems including weakly magnetic minerals such as hematite, goethite, pyrite, and montmorillonite. The late stage deposited minerals typical of vapor-dominated systems including low-magnetization minerals such as montmorillonite and some pyrite. Note that the presence of stable pyrite indicates a nonoxidizing environment in this part of the vapor-dominated system isolated from surface fluids. The presence of these secondary low-magnetization iron-bearing minerals suggests that this area (and also possibly the Smoke Jumper Hot Springs area) underwent significant demagnetization associated with hydrothermal alteration of the volcanic substratum.

Table 1 displays a range of values for remanent directions in the Lava Creek Tuff and the Scaup Lake Flow, possibly reflecting measurement errors, tectonic tilting, secular variation during cooling of the flow, effects of local magnetic anomalies associated with underlying rocks, or the presence of remanent overprints [Reynolds, 1977]. Both averaged remanent directions in the Lava Creek Tuff and the Scaup Lake Flow (deduced from Reynolds [1977]; Finn and Morgan [2002], and from our measurements) are relatively close to the direction predicted by a geocentric axial dipole (GAD), i.e., $I = 63^\circ$ and $D = 0^\circ$. Assuming for these units that the remanent magnetization approximates a GAD field direction, the induced magnetization is $I = 70^\circ$ and $D = 14^\circ$ (as predicted by the IGRF model), and the Q ratio is 10, leads to a total magnetization (sum of the induced and remanent magnetization vectors) that deviates less than 1° from the GAD direction. It is therefore reasonable to neglect the effect of induced magnetization in unaltered units and consider that magnetization of both the Lava Creek Tuff and the rhyolite flows is characterized by a GAD direction ($I = 63^\circ$ and $D = 0^\circ$) and an intensity of ~ 3 to 6 A/m. Note that our knowledge of the NRM intensity of the fresh volcanic units is still poorly

Table 2. Average Values of Standard Deviation of Magnetic Anomalies Computed in Overlapping Moving Windows Along the Ground Profiles for Areas 1–4 After Separating Portions of Profiles Inside and Outside Areas of Acid Hydrothermal Alteration (and Hydrothermal Deposits)^a

	Areas of Alteration			Areas of Alteration and Deposits		
	Standard Deviation (nT)		Ratio Outside/Inside	Standard Deviation (nT)		Ratio Outside/Inside
	Inside	Outside		Inside	Outside	
1 (Firehole River)	252.3	595.4	2.4	205.4	657.2	3.2
2 (Smoke Jumper Hot Springs)	93.0	154.4	1.7	93.0	154.4	1.7
3 (Norris Geyser Basin)	25.1	44.3	1.8	31.5	43.8	1.4
4 (Lone Star Geyser)	7.4	6.2	0.8	6.2	7.4	1.2

^aThe ratio of the average values obtained outside and inside these areas is also provided.

constrained since it is based exclusively on one study [Finn and Morgan, 2002] whose measurement sites are not necessarily representative of the overall units.

In the following analysis, we will also assume for simplicity that hydrothermal alteration results in the complete destruction of induced and remanent magnetizations of rhyolite flows and tuffs. Because hydrothermally altered units may be best characterized by a variable degree of demagnetization, our computations only provide the minimum extent of hydrothermal alteration. We also note that magnetic surveys may not allow us to detect all stages of hydrothermal alteration but only those that result in the destruction of magnetic minerals.

5. Ground Profile Analysis

5.1. Anomaly Amplitude

As mentioned above, the long magnetic traverses acquired across areas 1–3 reveal that short-wavelength anomaly amplitudes are lower over areas of hydrothermal alteration than over nearby unaltered areas. In order to quantitatively verify this observation, we estimated the averaged amplitude of short-wavelength anomalies by computing the standard deviation of magnetic anomalies over overlapping windows regularly spaced along the magnetic profiles (Figure 7). A linear trend was estimated and removed from the computation window before computing the standard deviation in order to remove effects of deeply sourced anomalies with wavelengths larger than the window width.

Figure 7 shows that, in study areas 1–3, the standard deviation of magnetic anomalies (i.e., amplitude of short-wavelength magnetic anomalies) is generally lower inside areas of hydrothermal alteration and deposits than outside. Indeed, Table 2 shows that averaged values of standard deviations evaluated inside areas of hydrothermal alteration (and deposits) are lower than outside these areas by a factor of about 2. This suggests that areas of hydrothermal alteration in YNP and other volcanic terrain could potentially be mapped by searching areas characterized by standard deviation of magnetic anomalies (i.e., averaged amplitude of short-wavelength anomalies) lower than a given threshold, provided that consideration is made for varying lithology, for example, which could influence the threshold from one area to another. Colored symbols in Figure 7 are underlain by a black thick line when standard deviations are below a threshold equal to half the averaged standard deviation observed outside areas of hydrothermal alteration or deposits (i.e., <330 nT for area 1 (Firehole river), <75 nT for area 2 (Smoke Jumper Hot Springs), and <20 nT for areas 3 (Norris Geyser Basin)).

Although areas of low standard deviation generally correlate well with mapped areas of hydrothermal alteration, some discrepancies are observed. Several areas of hydrothermal alteration do not display low standard deviations (See features SJ-A and SJ-B in area 2 Smoke Jumper Hot Springs and feature NG-A in area 3 Norris Geyser Basin). This may be due to a number of factors including the following: a computation window size that exceeds the size of alteration features (see features SJ-A and SJ-B), the proximity of unaltered areas that lie off-axis to the profile (see features SJ-A and NG-A), or possibly lower degrees of alteration. The low amplitude of short-wavelength anomalies in some cases extends beyond the edge of mapped hydrothermal areas (See feature SJ-C in area 2 Smoke Jumper Hot Springs and feature FR-A in area 1 Firehole River) suggesting that demagnetization due to hydrothermal alteration extends beyond the mapped area but is hidden under a thin cover of unaltered rocks, alluvium, or vegetation. Such areas could possibly be

areas of past hydrothermal activity that are now extinct. Feature FR-A suggests a continuous demagnetized zone instead of dispersed areas of hydrothermal alteration suggesting a much larger extent of alteration than the area mapped by *Christiansen and Blank* [1974].

The detailed survey acquired within area 4 also displays a zone of lower standard deviation (Figure 7d). This feature, however, does not correlate with the location of hydrothermal alteration and deposits. Indeed, averaged values of the standard deviation (Table 2) are similar inside and outside areas of hydrothermal alteration and deposits. Note, however, that limits of hydrothermal alteration and deposits are not very precisely mapped at this scale and the similar values obtained for standard deviation suggest that hydrothermal alteration occurs beyond these limits. The feature with low standard deviation approximately coincides with the location of the magnetic low centered on the Lone Star Geyser and other thermal features (marked by black triangles, see Figure 3b) and may therefore indicate an area of more pervasive alteration associated with the currently active vent.

5.2. Depth to Sources

The damping of short-wavelength anomalies observed along ground magnetic profiles can also be used to obtain a quantitative estimate of the depth to magnetic sources (i.e., the nonmagnetic terrain thickness). Many methods for estimating the depth to magnetic sources from magnetic intensity profiles exist [e.g., *Peters*, 1949; *Thompson*, 1982; *Reid et al.*, 1990; *Werner*, 1953; *Roest et al.*, 1992]. However, these methods rely on assumptions of the geometry of magnetic sources such as 2-D structures or specific geometries of the magnetic body (dipoles, lines of dipoles or sheets) or also require a regular spacing of data along profiles. Such assumptions are typically not met in the case of ground magnetic profiles and demagnetization associated with hydrothermal alteration. For this reason, we used a method proposed by *Smith* [1959] that makes no assumption of the geometry of magnetic sources or direction of magnetization. This method provides an upper bound on the depth to the source d of a magnetic anomaly observed on a total field anomaly profile $\Delta T(x)$ (Figure 8). *Smith* [1959] provides two relationships for the limiting depth based on the maximum value of the first or second derivatives of the field anomaly profile, $|d\Delta T/dx|_{max}$ (in nT/m) and $|d^2\Delta T/dx^2|_{max}$ (in nT/m²), and on the maximum contrast of magnetization intensity M_{max} (in A/m) between the causative body and a homogeneous substratum. We used here the relationship based on the first derivative of the anomaly profile, as this quantity is likely better constrained than the second derivative:

$$d \leq 628 \left(4\hat{b}_x^2 + 3\hat{b}_y^2 + 3\hat{b}_z^2 \right)^{1/2} \frac{M_{max}}{|d\Delta T/dx|_{max}} \quad (1)$$

where $\hat{b} = (\hat{b}_x, \hat{b}_y, \hat{b}_z)$ is a unit vector in the direction of the regional field whose components are defined in a local reference frame (x, y, z) , with x oriented in the direction of the magnetic profile. Our ground magnetic profiles are not straight (see Figures 2 and 3) and the orientation of the frame (x, y, z) changes along the profile. Nevertheless, for simplification, the root-square term in equation (1), whose value is between $\sqrt{3}$ and 2, was replaced by its maximum value 2. As a consequence, there may be a slight directional effect in the limiting depth obtained from this simplified relationship. However, we will see that this effect is small compared to the observed variations that cover several orders of magnitude.

Note that because the method of *Smith* [1959] only gives an upper bound on the depth to source d , obtained depths may be larger than real depths to sources. However, *Fedi and Florio* [2013] recently tested similar formulas for limiting depths predicted by *Bott and Smith* [1958] for the gravity field and showed that these formulas provide correct depths in the case of point and line sources and consistent estimates for general sources. We therefore use the *Smith* [1959] method to provide an order of magnitude estimate of the depth to magnetic sources, keeping in mind that obtained depths may be larger than real depths to magnetic sources.

As the ground magnetic profile contains a certain amount of noise (with respect to position or magnetic intensity), we first fitted splines of order 5 (with a break spacing of 2 m and a minimum number of two data points between breaks) to the profiles before estimating its first derivative. Then, because a fresh volcanic substratum is likely to contain numerous magnetization intensity contrasts and therefore many associated magnetic anomalies, we performed an automated search for local maxima of the first derivative $|d\Delta T/dx|_{max}$. This yielded a large number and range of limiting depths including very large values associated with deep sources in the volcanic substratum. We assumed that constraints on the depth to the bottom of the

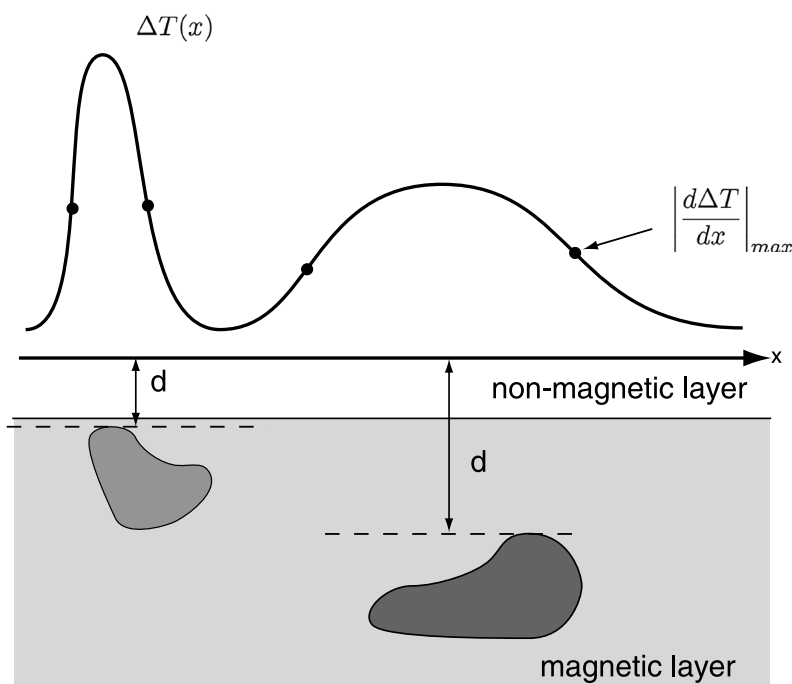


Figure 8. Sketch showing a magnetic anomaly profile, $\Delta T(x)$, acquired over a nonmagnetic layer underlain by a magnetic layer containing several bodies characterized by different magnetization intensity (darker grey corresponding to larger magnetization). The maximum value of the first spatial derivatives (located by black dots) along the profile provides a maximum estimate for the depth to the top, d , of the causative magnetic body. The minimum value of d obtained using a large range of magnetic anomalies may provide an estimate of the depth to the top of the magnetic layer.

nonmagnetic or demagnetized layer overlying the fresh volcanic substratum may be best obtained from the lowest values of the limiting depth (Figure 8). For this reason, we eliminated large values of limiting depths moving a five-point window over the profile and retaining for each window only the lowest value.

The appropriate value for the maximum contrast of magnetization intensity M_{\max} is difficult to constrain. It cannot be larger than the maximal magnetization intensity within the unit (i.e., $\sim 3\text{--}6 \text{ A/m}$, assuming our rock sample measurements are representative of the fresh substratum magnetization), and it probably has a different value in the three investigated areas as these areas are characterized by different anomaly amplitudes over unaltered units. As we expect a minimum distance between magnetic sources and the magnetic sensor of $\sim 2 \text{ m}$ (sensor height above ground) in areas where the unaltered volcanic substratum is at the surface, we searched in areas 1–3 for the value of M_{\max} that provides a minimum value for the limiting depth of 2 m (i.e., 2.2 A/m for area 1 (Firehole River), 0.2 A/m for area 2 (Smoke Jumper Hot Springs), and 0.4 A/m for area 3 (Norris Geyser Basin)). Because area 4 is a subset of area 3, we used the same value for M_{\max} (i.e., 2.2 A/m) for both areas.

Figure 9 shows the resulting map of limiting depths estimated in study areas 1–4. As expected, shallow magnetic sources are observed in unaltered volcanic terrain. In contrast, areas of hydrothermal alteration are characterized by larger depths to magnetic sources, with maximum values varying from $\sim 100 \text{ m}$ (in area 2, Smoke Jumper Hot Springs) to $\sim 1000 \text{ m}$ (in areas 1, Firehole River, and 3, Norris Geyser Basin). The larger magnetic gradient and lower limiting depths obtained in area 2 may indicate that hydrothermal alteration extends over a shallower zone in this area but it could also be explained by the proximity of unaltered areas on the sides of the hydrothermal zone. Indeed, whereas hydrothermal activity and alteration are distributed over a few thousand meter wide zones over areas 1 and 3, they occur along relatively narrow linear zones of a few hundred meters wide over area 2. Therefore, the assumption of a horizontal nonmagnetic layer of infinite extension underlain by a magnetic layer as represented in Figure 8 is not valid in area 2.

Furthermore, an alternative interpretation of Figure 9 could be that lower values of magnetic gradient $|d\Delta T/dx|$ observed in areas of hydrothermal alteration are due to a decrease of magnetization intensity contrasts M_{\max} due to partial demagnetization of the shallow substratum. The estimated limiting depths of 100 m–1000 m in

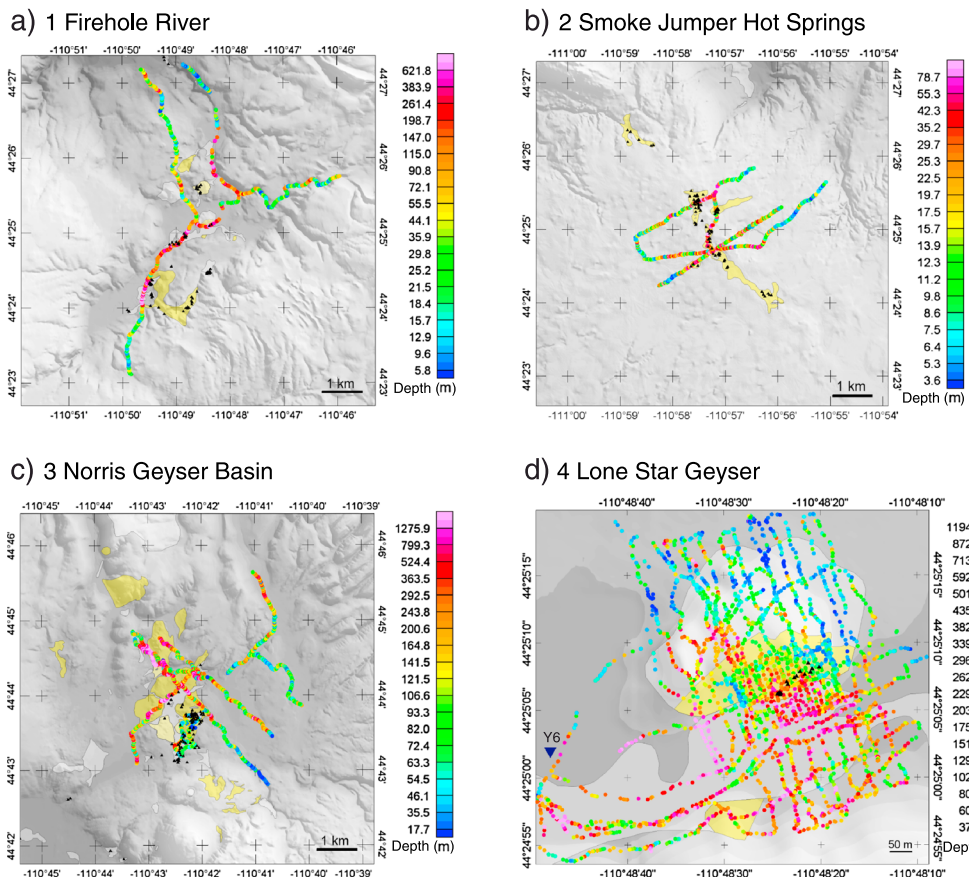


Figure 9. Maximum depth of magnetic sources deduced from the maximum values of the first spatial derivative along the ground magnetic profiles in study areas 1–4: (a) Firehole River, (b) Smoke Jumper Hot Springs, (c) Norris Geyser Basin, and (d) Lone Star Geyser. Estimates are obtained assuming a maximum contrast of magnetization intensity M_{\max} of 2.2 A/m (for areas 1 and 4), 0.2 A/m for area 2, and 0.4 A/m for area 3. Depth estimates have been decimated by retaining only the lowest depth over moving window of five estimates. Areas of acid hydrothermal alteration and hydrothermal deposits are indicated by yellow and white polygons, respectively. Thermal features are represented by black triangles. These symbols are represented over shaded topography in the background. Note that the color scale is different for each area.

altered areas (compared to depths of 2 m in unaltered areas, see Figure 9) could instead indicate that shallow magnetization intensity contrasts are reduced by a factor of 50 to 500.

The detailed survey in area 4 (Figure 9d) shows anomalously large depths to magnetic sources that coincide with the location of the geyser and thermal springs and extend along the river. This feature is crossed by several profiles that show a similar depth range, confirming that it has real geophysical significance. The origin of this feature could be a deeper extent of hydrothermal alteration in this area or instead a shallow zone of complete demagnetization within a partially demagnetized substratum characterized by a lower value of M_{\max} than the fresh volcanic substratum outcropping in area 1 (Firehole River). Thickness of river sediments may also partly account for the deeper depths.

6. Inversion

The *Smith* [1959] method provides only an estimate of the maximum possible value for the depth to the top of magnetic sources below the profile path. In order to more precisely determine the distribution of magnetic sources over the entire study area, while taking into account topography, we rely on inverse methods derived from the *Parker* [1972] method for rapid calculation of magnetic anomalies associated with topography. These calculations are performed in the Fourier domain and assume that magnetic

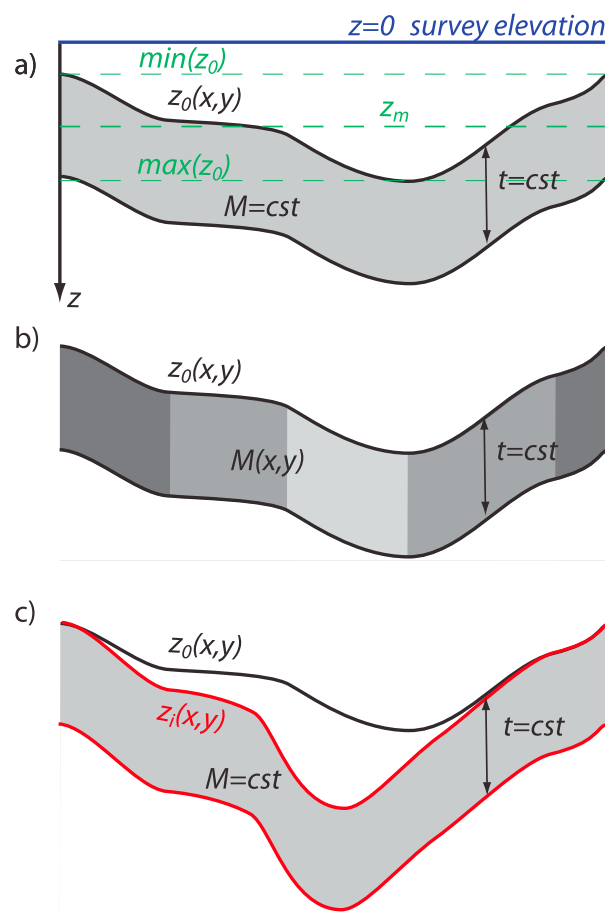


Figure 10. Three sets of assumptions used to reproduce the total field magnetic anomalies $\Delta T(x,y)$ observed on a horizontal plane: (a) constant magnetization M in a layer of constant thickness t below the topography $z_0(x,y)$, (b) horizontal variations of the magnetization intensity $M(x,y)$ in a layer of constant thickness t below the topography $z_0(x,y)$, and (c) constant magnetization M in layer of constant thickness t below a magnetic topography $z_1(x,y)$ different from the real topography $z_0(x,y)$. Notations $M = cst$ and $t = cst$ mean these parameters are constant. z_m is defined as the midvalue of the topography $z_0(x,y)$.

anomalies are measured on a horizontal surface. We apply these methods to both the high-resolution aeromagnetic survey in areas 1–3 and the detailed ground survey in area 4. Since these surveys are draped above the ground (height of roughly 250 m for the aeromagnetic survey; constant height of 2 m above the ground for the ground survey), we first upward continue these grids to a horizontal surface of constant elevation using the “Chessboard” method from Cordell [1985]. With this method, the grid measured on an irregular surface is first upward continued on parallel surfaces using the standard level-to-level transformation. The resulting grids are then used to interpolate a new grid on a constant elevation level. Although necessary, such upward continuation implies approximations as level-to-level transformation is applied to data acquired on an irregular surface. It also attenuates the short-wavelength anomalies resulting in a loss of resolution.

In the following, the upward continued grids are first compared with magnetic anomalies predicted assuming a constant substratum magnetization and second used to invert the distribution of magnetization in the substratum.

6.1. Topographic Effect

In order to discriminate between magnetic anomalies due to topography and magnetic anomalies due to geological contacts or hydrothermal alteration, we first compute maps of the magnetic anomaly (noted $\Delta T(x,y)$) produced by the topography (noted $z_0(x,y)$) assuming that the magnetization direction and intensity are constant within a half-space below topography. This computation is performed using the Parker [1972]

Table 3. Results of the Search for the Magnetization Parameters That Provide the Minimum Correlation Coefficient Between Residual Anomaly and Topography in Areas Qpcs-1 (a), Qpcs-2 (b), and Qylb (c), Whose Locations Are Indicated by Brown Squares in Figure 1: Magnetization Declination D , Inclination I and Intensity M , Correlation Coefficient, and Relative RMS (i.e., Ratio of the RMS of Residual Anomalies Over the RMS of Observed Anomalies)^a

Area	D (deg)	I (deg)	M (A/m)	Correlation Coefficient	Relative RMS (%)
Qpcs-1	0	63	4.9	3.E-03	91
	4	58	5.3	2.E-06	93
Qpcs-2	0	63	1.8	1.E-02	76
	9	68	1.7	-4.E-06	77
Qylb	0	63	1.7	-3.E-03	81
	-6	52	2.0	-7.E-06	79

^aFor each area, the first line is obtained by setting the magnetization direction to be that of the GAD field and searching for the magnetization intensity, the second line is obtained by searching for both the magnetization direction and intensity.

method presented here for a layer of constant thickness t below topography (Figure 10a; t tends to infinity for a half-space) and using notations similar to Blakely [1995]

$$\mathcal{F}(\Delta T) = 2\pi C_m \theta_m \theta_b e^{-|\vec{k}| z_m} \left(1 - e^{-|\vec{k}| t}\right) \sum_{n=0}^{\infty} \frac{(-|\vec{k}|)^n}{n!} \cdot \mathcal{F}(M(z_0 - z_m)^n) \quad (2)$$

where \mathcal{F} indicates Fourier transform. We used a fast Fourier transform algorithm after subtracting the averaged value of the grid, expanding its size to the next power of 2 in both directions, and applying a Hanning taper along each side. $C_m = 10^{-7}$ SI is a proportionality constant, M is the magnetization intensity, z_m is the midvalue between the maximum and minimum values of $z_0(x, y)$, $\vec{k} = (k_x, k_y)$ is the wave vector, k_x and k_y are wave numbers in the x and y directions, and θ_m and θ_b are factors that take into account magnetization and magnetic field directions. The factors θ_m and θ_b are defined as

$$\theta_m = \hat{m}_z + i \frac{\hat{m}_x k_x + \hat{m}_y k_y}{|\vec{k}|}$$

$$\theta_b = \hat{b}_z + i \frac{\hat{b}_x k_x + \hat{b}_y k_y}{|\vec{k}|}$$

with \hat{m} and \hat{b} , unit vectors in the direction of the magnetization and of the magnetic field, respectively. The x axis is oriented toward north, the y axis toward east, and the z axis is positive in the downward direction; the origin coincides with the survey elevation. Thus, $z_0(x, y)$ is defined as the distance between the survey elevation and topography. The summation over n in equation (2) is performed until the ratio of the energy in the n th term (sum over all values of \vec{k} of the norm of the n th term) over the energy of all previous terms is lower than 10^{-3} . The subtraction of z_0 by its midvalue z_m is introduced to provide fast convergence of the summation. Indeed, convergence may not always be attained. However, Parker [1972] showed that convergence of this summation is expected if the term $e^{-|\vec{k}| z_m}$ is put inside the sum and if the ratio of the topography amplitude over the distance between the survey and the topography (i.e., $\max|z_0 - z_m|/z_m$) is smaller than 1. Such condition is always ensured as z_m is defined as the midvalue of the topography $z_0(x, y)$ and as the survey elevation lies above the topography (see Figure 10a). However, convergence will be slower if the ratio $\max|z_0 - z_m|/z_m$ is closer to 1, i.e., a larger number of iterations will be needed for ground magnetic data than aeromagnetic data. Equation (2) is used only for $|\vec{k}| \neq 0$ and we imposed the Fourier transform of magnetic anomalies to be zero at $|\vec{k}| = 0$, as magnetic anomalies average to zero over the space domain.

This computation requires a priori knowledge of the magnetization intensity and direction representative of the overall study area. Some constraints can be obtained from laboratory measurements on rock samples (see section about rock properties). However, since these measurements are restricted to only a few samples collected near the surface or within a few drill cores, we do not know if their magnetic properties are representative of the bulk properties of the substratum. An independent estimate of the substratum magnetization can be obtained by searching for the magnetization direction and intensity that best reproduce magnetic anomalies due to topography. Such was done for instance by Francheteau *et al.* [1970] and Blakely and Christiansen [1978], relying, however, on a different method than the present study for the

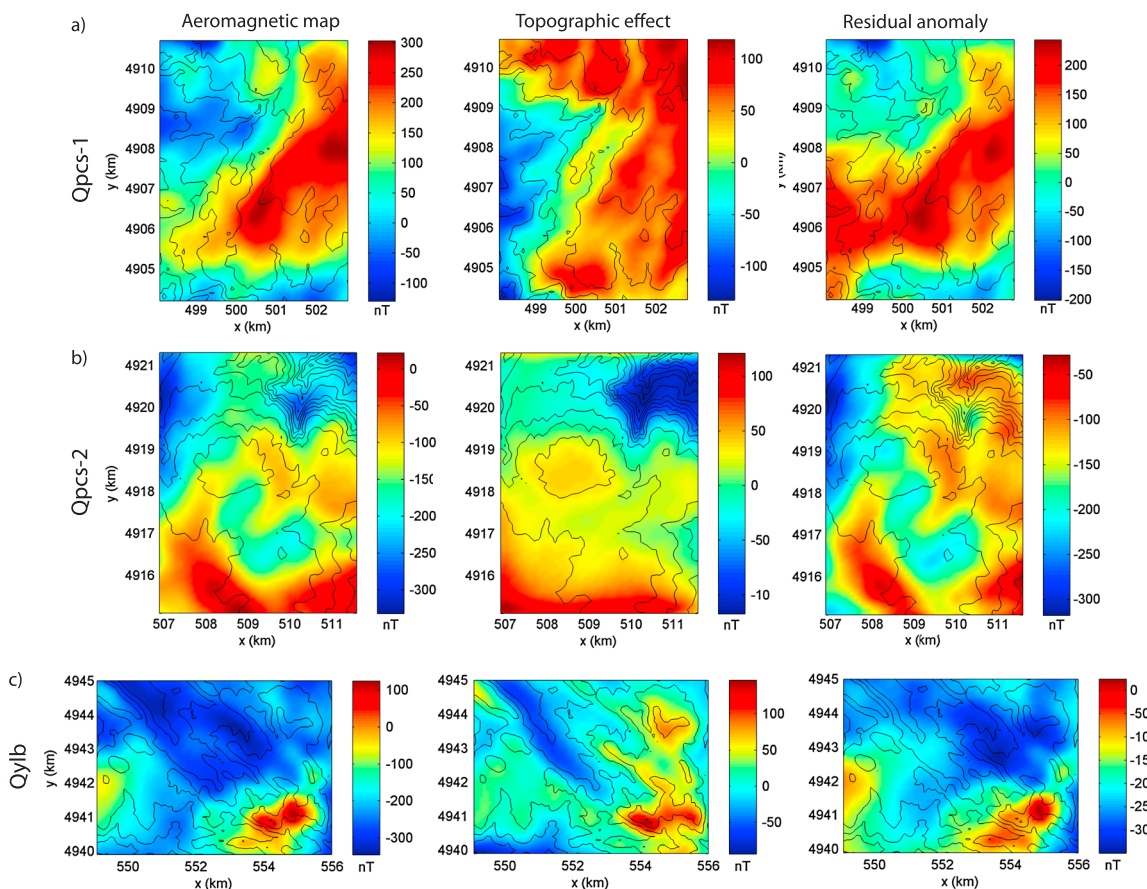


Figure 11. Observed total field anomaly (left column), topographic effect (middle column), and residual anomaly (right column) for areas (a) Qpcs-1, (b) Qpcs-2, and (c) Qylb, whose locations are indicated by brown squares in Figure 1. Maps are presented at a constant elevation level of 2827 m for Qpcs-1, 2877 m for Qpcs-2, and 2999 m for Qylb. Topographic effects are computed assuming a constant magnetization with a GAD field direction and intensities of 4.9 A/m, 1.8 A/m, and 1.7 A/m, respectively (intensity providing a minimum correlation between residual anomaly and topography). Black lines are topographic contours represented with a 20 m spacing (Figures 11a and 11b) and a 50 m spacing (Figure 11c).

computation of magnetic anomalies due to topography [e.g., *Talwani*, 1965]. In practice, this type of estimate is difficult because it requires that magnetization be constant within the entire investigated area, which is generally not the case, and because variations of magnetization can bias the results [*Blakely and Christiansen*, 1978]. Our selected study areas are therefore not ideal because they display magnetic lows associated with hydrothermal alteration suggesting demagnetization of the substratum. In order to gain additional information about the magnetization of the fresh geological units outcropping in our study areas, we selected a few regions (see brown squares in Figure 1) composed only of the geological unit of interest, displaying no hydrothermal alteration or deposits, and showing magnetic anomalies correlated with topography. In practice, only a few areas passed these three criteria. In particular, several areas do not display anomalies correlated with topography, suggesting either a low magnetization of the shallow volcanic substratum or large variations in magnetization producing anomalies that hide anomalies associated with topography. The three selected areas are the following: areas Qpcs-1 and Qpcs-2, both composed of the Summit Lake rhyolite flow (outcropping in area 2, Smoke Jumper Hot Springs), and area Qylb, composed of the Lava Creek Tuff (outcropping in area 3, Norris Geyser Basin). Area Qylb is remote from area 3 because we did not find any closer area suitable for the parameter search. As a consequence, significant variations in the magnetic properties of the tuffs may exist between area Qylb and area 3.

In order to find the best magnetization intensity and direction, we performed two different experiments. In the first experiment, we set the magnetization direction to be that of the GAD field and let the intensity vary, whereas in the second experiment, we let both the magnetic direction and intensity vary. These parameters are sampled within ranges of realistic values that include values displayed in Table 1 (every 0.1 A/m between 0

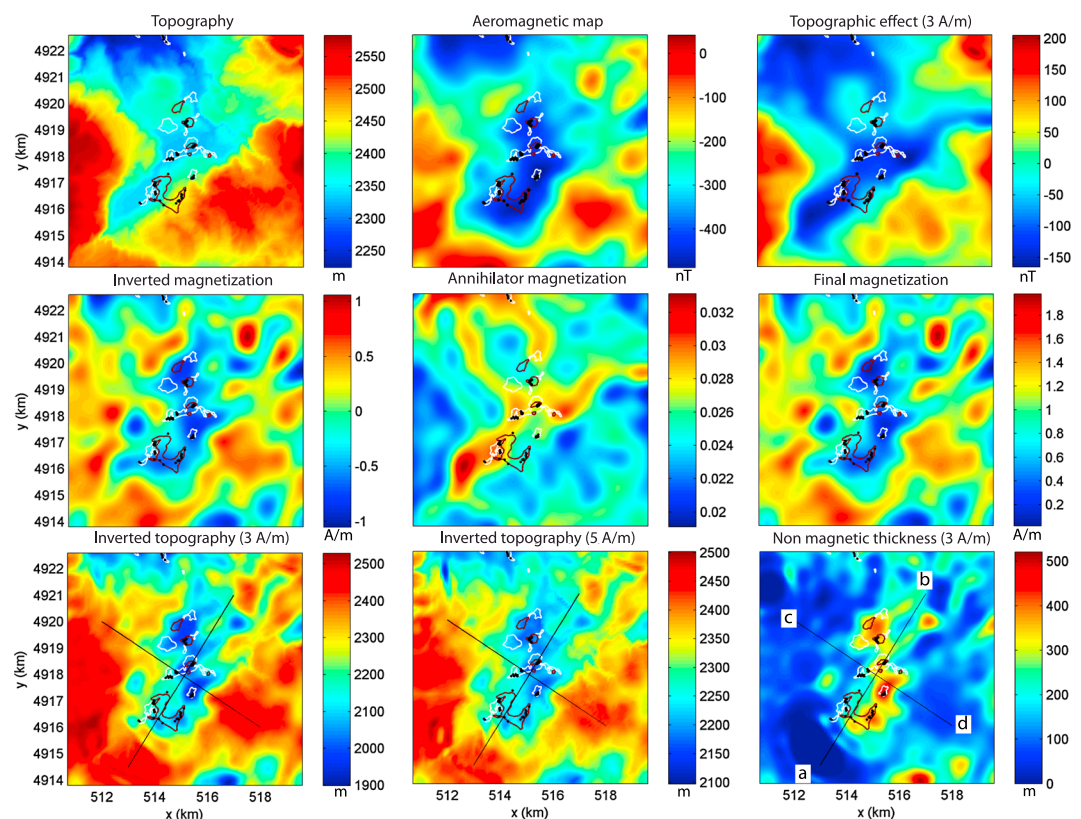


Figure 12. Set of maps for area 1 (Firehole River) presented at a constant elevation level of 2855 m (from left to right and top to bottom): topography, observed aeromagnetic anomaly (not reduced to the pole), topographic effect computed assuming a constant magnetization of 3 A/m and using (2), inverted magnetization M computed using (3), annihilator magnetization a computed using (6), final magnetization $M + aa$, inverted topography computed assuming a constant magnetization of 3 A/m or 5 A/m and using (7), and nonmagnetic thickness computed assuming a constant magnetization of 3 A/m. Magnetization direction is assumed to be those of a GAD field. Areas of acid hydrothermal alteration and hydrothermal deposits are indicated by brown and white thick lines, respectively. Thermal springs are located by black dots. Letters on the bottom right plot are endpoints of cross sections represented in Figure 16.

and 10 A/m for the intensity, every degree between -20° and $+20^\circ$ for the declination, and every degree between 50° and 80° for the inclination). For each set of parameters, we predict the anomaly grid produced by topography and subtract this grid from the observed anomaly grid. We then search for the parameters that provide a residual magnetic anomaly grid whose correlation coefficient with topography is minimal as is done for gravity anomalies within the Nettleton [1939] method. Note that there is a slight shift and distortion of magnetic anomalies produced by topography because of the magnetization and ambient field directions which are not vertical and this could partly bias our estimation.

Results of these searches are shown in Table 3. A comparison of the observed anomalies, topographic effects, and residual anomalies assuming a GAD direction for magnetization is presented in Figure 11. In the three investigated areas, the topographic effect reproduces relatively well some but not all of the observed anomalies. The residual anomaly maps still display large-amplitude anomalies, as reflected in root-mean-square (RMS) values of residual anomalies that range between 75% and 95% of the RMS of observed anomalies (Table 3). These residual anomalies indicate that the magnetization parameters may not always be accurately recovered, possibly because of the neighboring nontopographical anomalies (e.g., contrasts of magnetization in the substratum) that may bias the parameters search. Nevertheless, magnetization intensity seems relatively well constrained in these areas as similar estimates are obtained from the two experiments (both with a fixed or adjustable magnetization direction).

Magnetization intensities deduced from topographic effects ($\sim 2\text{--}5$ A/m for rhyolite flows and ~ 2 A/m for tuffs) are in the same range as estimates obtained from laboratory measurements (3 A/m for rhyolite flows and 6 A/m

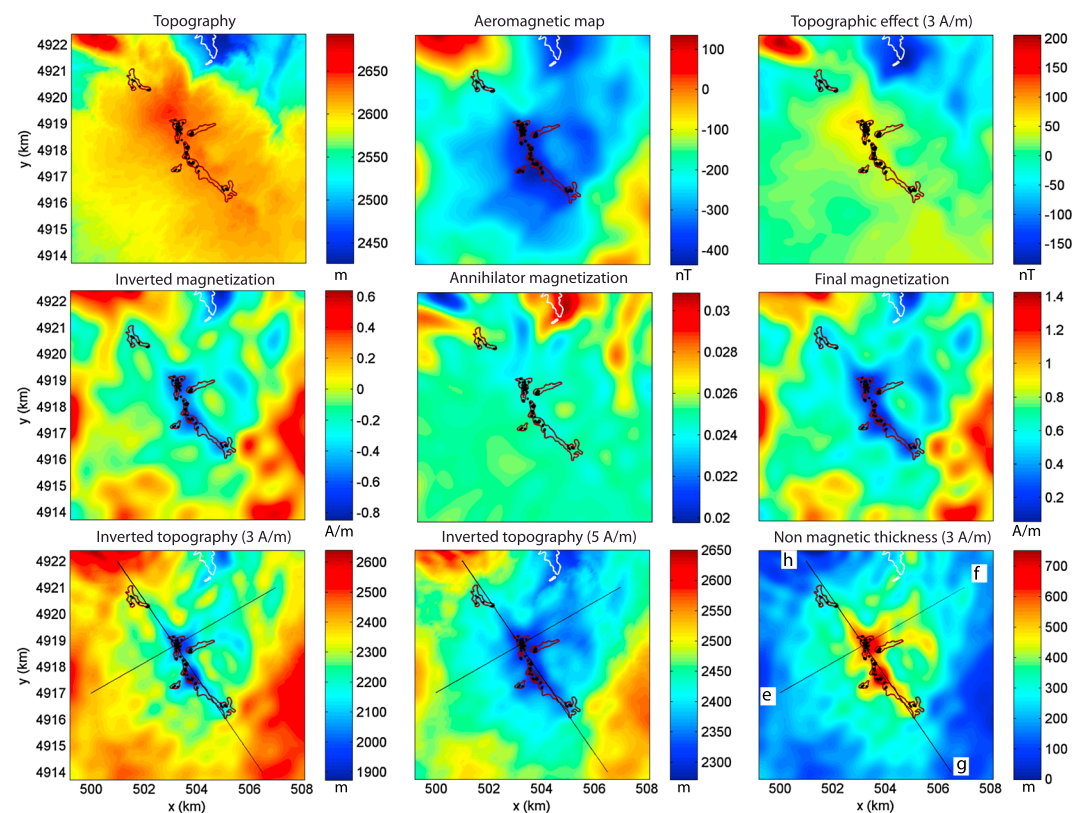


Figure 13. Set of maps for area 2 (Smoke Jumper Hot Springs) presented at a constant elevation level of 2940 m. Same legend as in Figure 12.

for tuffs). Estimated magnetization directions are relatively close to those of a GAD field (differences in inclination and declination less than $\sim 10^\circ$). In the following models, we will assume that magnetization direction is that of a GAD field. Because large uncertainties remain with respect to magnetization intensity of the fresh substratum, we will consider two intensity values: 3 and 5 A/m.

Topographic effects in areas 1–4, computed assuming a constant magnetization of 3 A/m with a GAD field direction ($I = 63^\circ, D = 0^\circ$) in a half-space below topography, are represented on the top right plots of Figures 12–15. These maps reproduce some but not all observed anomalies. The topographic anomaly map computed in area 1 (Firehole River, Figure 12) displays a central negative anomaly at the same location but with a different shape than the observed negative anomaly correlated with hydrothermal features, indicating that the observed negative anomaly is due both to topography and contrasts of magnetization. The positive and negative anomalies at the north edge of area 2 (Smoke Jumper Hot Springs, Figure 13) are well reproduced by topographic anomalies showing that they are not due to variations in the magnetization of the substratum. On the other hand, the negative anomaly correlated with hydrothermal alteration in area 2 is not reproduced in the topographic anomaly map and is therefore indeed associated with a contrast of magnetization. Larger anomaly values at the east and west edges of area 3 (Norris Geyser Basin, Figure 14) may be due to topography as larger values are also observed in the topographic anomaly map. Finally, no correlation is observed in area 4 (Lone Star Geyser, Figure 15) between observed and topographic anomalies suggesting the substratum beneath topography has a low or null magnetization. This is consistent with its location in the altered zone of area 1. Table 4 shows that smaller RMS of differences between observed and topographic anomaly maps and lower correlation coefficients between residual anomaly and topography maps is obtained assuming a magnetization intensity of 3 A/m rather than 5 A/m suggesting that magnetization over our study areas is closer to 3 A/m than 5 A/m.

6.2. Inversion of Equivalent Magnetization

Next, we use the *Parker and Huestis* [1974] method, frequently used for interpreting marine magnetic anomalies, to estimate the equivalent magnetization of the substratum assuming that magnetization is confined to a layer

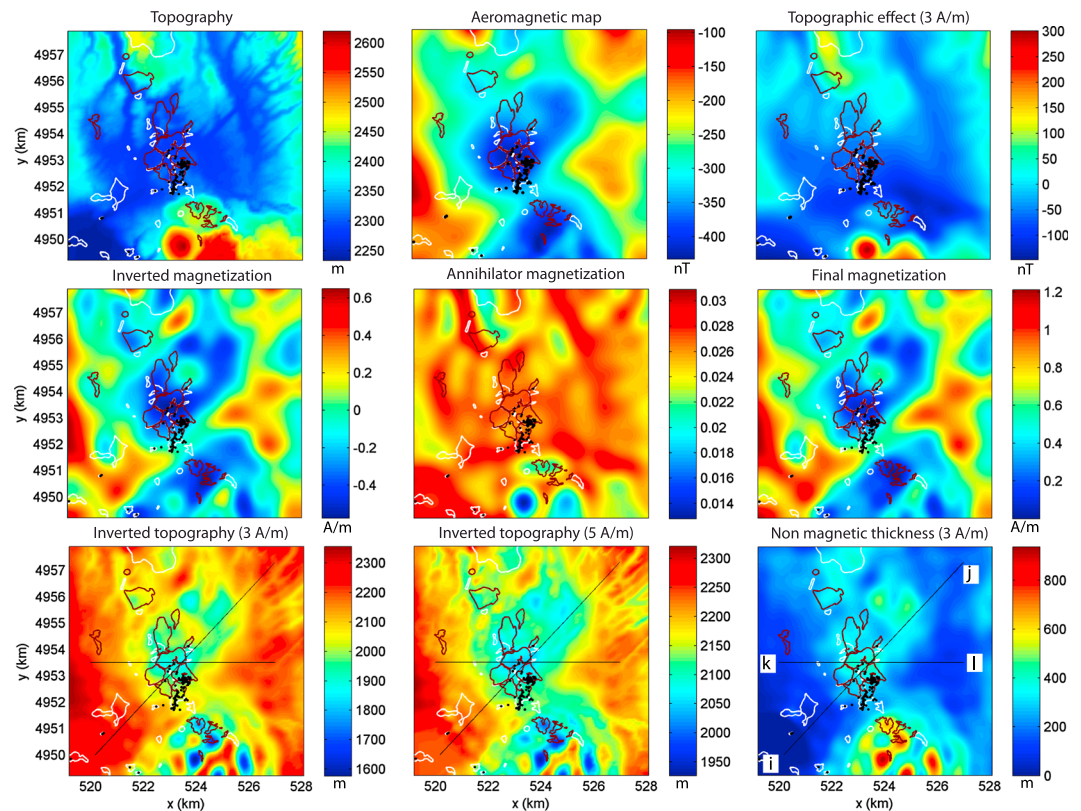


Figure 14. Set of maps for area 3 (Norris Geyser Basin) presented at a constant elevation level of 2885 m. Same legend as in Figure 12.

of constant thickness below topography, magnetization direction is constant and coinciding with a GAD field direction ($I = 63^\circ$, $D = 0^\circ$), and magnetization intensity varies only in horizontal directions (x, y) and is constant in the vertical direction (z) (Figure 10b). Inherent in our application of this method is the assumption that demagnetization associated with hydrothermal alteration is confined into vertical pipes in the shallow subsurface.

Formula (2) is also valid if M is not constant but varies in the horizontal direction (with x and y). Therefore, the Parker and Huestis [1974] method is simply derived from the Parker [1972] method by isolating the $n = 0$ term of the summation in equation (2):

$$\mathcal{F}(M) = \frac{\mathcal{F}(\Delta T)}{2\pi C_m \theta_m \theta_b e^{-|\vec{k}| z_m} (1 - e^{-|\vec{k}| t})} - \sum_{n=1}^{\infty} \frac{(-|\vec{k}|)^n}{n!} \mathcal{F}(M(z_0 - z_m)^n) \quad (3)$$

This equation contains the magnetization intensity M both in its right and left sides. Therefore, magnetization intensity is estimated by iteration, starting from an a priori model, $M_0(x, y)$, which was in our case a constant value of 1 A/m, and repeated until the i th iteration when the ratio of the norm of the increment $M_i(x, y) - M_{i-1}(x, y)$ to the norm of $M_i(x, y)$ is lower than 10^{-3} . The spectral content of magnetic anomalies is in general relatively poorly constrained at high wave numbers (short wavelengths) for which the signal to noise ratio is low. Each iteration of equation (3) tends to amplify these poorly constrained wave numbers, since $\mathcal{F}(\Delta T)$ is divided by a very small quantity $e^{-|\vec{k}| z_m}$ for high values of $|\vec{k}|$ (as $z_m > 0$). For this reason, we tapered the large wave numbers of the magnetization with a smooth low-pass filter following Schouten and McCamy (1972):

$$\begin{aligned} k \leq k_h - w_h & \quad B(k) = 1 \\ k_h - w_h < k < k_h & \quad B(k) = \frac{1}{2} \left(1 - \cos \left[\pi \frac{k - k_h}{w_h} \right] \right) \\ k_h \leq k & \quad B(k) = 0 \end{aligned} \quad (4)$$

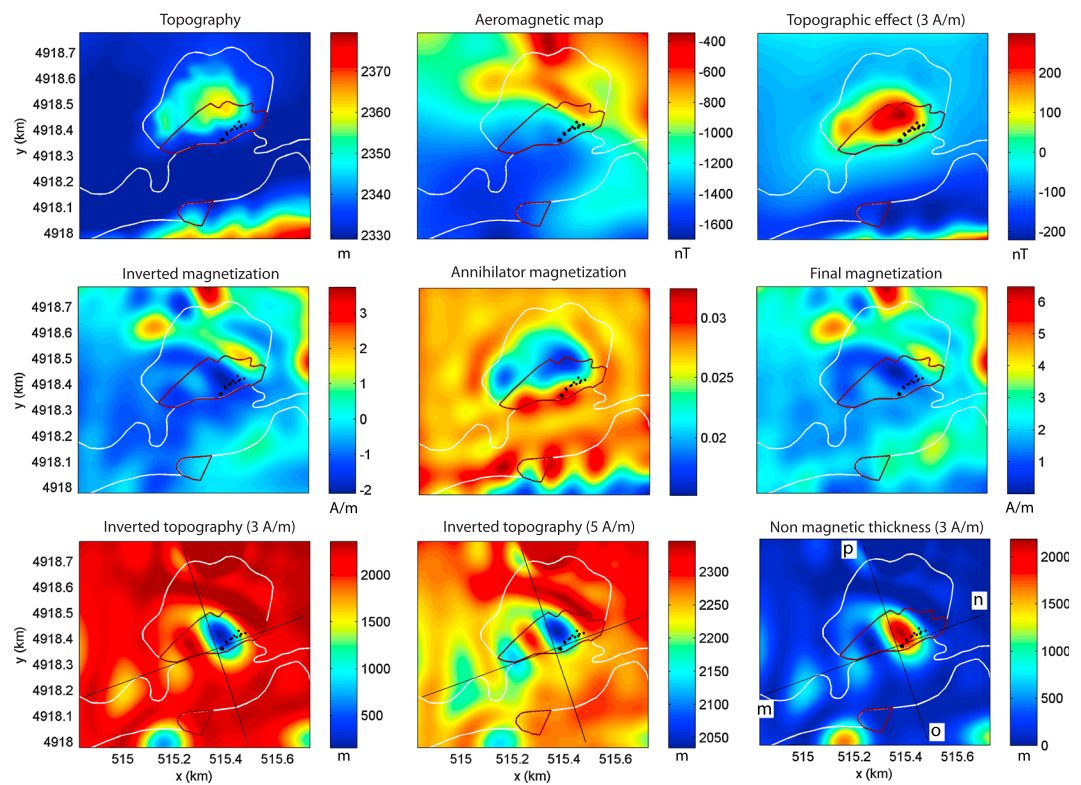


Figure 15. Set of maps for area 4 (Lone Star Geyser) presented at a constant elevation level of 2402 m. Same legend as in Figure 12.

where k_h is the wave number cutoff point and w_h is the width of the taper. These parameters were first chosen according to the shape of the radial power spectrum of magnetic anomalies as defined in Bouligand *et al.* [2009] and second, empirically adjusted to allow the highest spatial resolution without unrealistic amplification of unconstrained short wavelengths: $k_h = 8 \times 10^{-3}$ rad/m (i.e., a wavelength of ~ 790 m) and $k_h - w_h = 3 \times 10^{-3}$ rad/m (i.e., ~ 2100 m) for aeromagnetic data in areas 1–3 and $k_h = 5 \times 10^{-2}$ rad/m (i.e., ~ 130 m) and $k_h - w_h = 4 \times 10^{-2}$ rad/m (i.e., ~ 160 m) for ground data in area 4.

Because of the nonuniqueness associated with potential field problems, the magnetization grid obtained after iterations of formula (3) is not the only magnetization distribution consistent with the magnetic anomaly map. For each study area, we can calculate an annihilator (i.e., a distribution of magnetization that does not produce any magnetic anomaly) which is consistent with our assumptions (magnetization constant in the z direction) and with the presence of topography. As shown by Parker and Huestis [1974], the

Table 4. Parameters and Results of the Topographic Effect Computation in Areas 1–4 Performed Using (2) and Assuming a GAD Field Direction: Magnetization Intensity of the Substratum M Used for the Computation, RMS of Differences Between Observed and Topographic Anomaly Maps, and Correlation Coefficient Between Residual Anomaly and the Topography Maps

Zone	M (A/m)	RMS (nT)	Correlation Coefficient
Firehole River	3	77.0	0.13
	5	94.8	-0.40
Smoke Jumper Hot Spring	3	91.1	-0.27
	5	100.5	-0.50
Norris Geyser Basin	3	86.3	-0.56
	5	114.9	-0.65
Lone Star Geyser	3	298.1	-0.07
	5	308.8	-0.15

Table 5. Parameters and Results of the Magnetization Inversion in Areas 1–4 Performed Using (3) and (6) and Assuming a GAD Field Direction: Thickness of Magnetic Layer ($+\infty$ Corresponding to a Half-Space), Amount α of the Annihilator Added in the Final Magnetization Map αa , RMS of Magnetic Anomalies Produced by the Added Annihilator's Magnetization Distribution αa , RMS of Differences Between Observed Magnetic Anomalies and Final Model Predictions, and Maximum Value of Magnetization Obtained Over the Study Area

Zone	Thickness t (m)	α (A/m)	Annihilator RMS (nT)	Magnetization RMS (nT)	Max. Magnetization (A/m)
Firehole River	500	75.9	2.9	5.6	3.4
	$+\infty$	37.8	1.5	5.7	2.0
Smoke Jumper Hot Spring	500	70.2	1.7	3.9	3.3
	$+\infty$	29.9	0.8	3.7	1.4
Norris Geyser Basin	500	54.3	1.8	2.3	2.8
	$+\infty$	23.3	0.8	2.3	1.2
Lone Star Geyser	500	101.2	2.6	8.1	6.6
	$+\infty$	100.3	2.6	8.1	6.5

annihilator, noted $a(x, y)$, can be derived from formula (3) with the first term on the right-hand side of the equation replaced by $\delta(k_x)\delta(k_y)$, δ being the Dirac function

$$\mathcal{F}(a) = \delta(k_x)\delta(k_y) - \sum_{n=1}^{\infty} \frac{(-|\vec{k}|)^n}{n!} \mathcal{F}(a(z_0 - z_m)^n) \quad (5)$$

which is equivalent to

$$a = \frac{1}{4\pi^2} \cdot \mathcal{F}^{-1} \left(\sum_{n=1}^{\infty} \frac{(-|\vec{k}|)^n}{n!} \mathcal{F}(a(z_0 - z_m)^n) \right) \quad (6)$$

The annihilator can therefore be computed through iterations of formula (6) starting with an initial model, chosen here to be a constant value of 0. Any amount α of the annihilator can be added to the magnetic distribution without affecting the fit between calculated and observed anomalies. In other words, $M(x, y)$ and $M(x, y) + \alpha a(x, y)$ fit the observed magnetic anomaly equally well. In order to estimate the proper value for α of annihilator to add, we imposed the restriction that the minimum value of magnetization observed over the study areas is equal to zero. This amounts to assuming that hydrothermal alteration leads to the complete demagnetization of the substratum and that there is no reverse magnetization. Note that the annihilator defined in (6) is nondimensional and the unit of α is therefore in A/m.

Maps of the inverted magnetization $M(x, y)$, the annihilator $a(x, y)$, and the final magnetization $M(x, y) + \alpha a(x, y)$ in areas 1–4, shown on the central row of Figures 12–15, were obtained assuming magnetization is constant in the vertical direction in a half-space below topography and has a GAD field direction ($I = 63^\circ$, $D = 0^\circ$). In the four areas, the lowest magnetization values generally coincide with hydrothermal activity or alteration. Moreover, in areas 1 and 2 (Figures 12 and 13), the shape of the low-magnetization zone is very similar to the shape of superficial hydrothermal features. The addition of a given amount α (see Table 5) of the annihilator shifts the minimum value of magnetization to zero but introduces only slight changes to the shape of features observed in the magnetization distribution. Table 5 shows that magnetic anomalies produced by the added annihilator αa are negligible (RMS < 3 nT), and differences between observed anomalies and model prediction are also very small (RMS < 10 nT) in comparison with anomaly amplitudes observed over the studied areas (~ 400 nT). Models obtained assuming a magnetic substratum consisting of a half-space or a 500 m thick layer (not represented in Figures 12–15) agree equally well with the observed anomaly (similar values of RMS in Table 5). We observe that magnetization distributions obtained assuming a half-space display narrower zones of decreased magnetization and smaller contrasts of magnetization intensity between altered and unaltered substratum in comparison with a 500 m layer model (not shown in Figures 12–15): maximum magnetization of ~ 1 A/m for a half-space versus ~ 3 A/m for a 500 m thick layer in areas 1–3 and maximum magnetization of ~ 6 A/m for both cases in area 4 (see Table 5). The larger maximum magnetization obtained in area 4 may simply be due to the use of a low-pass filter with a higher wave number cutoff for ground magnetic data (wavelength cutoff of ~ 100 m for ground data versus

~500 m for aeromagnetic data). For this reason, magnetization estimates represent averaged values of the magnetization distribution over smaller surfaces for ground magnetic data than aeromagnetic data. The similar value for the maximum magnetization observed over area 4 for both a half-space and a 500 m thick layer model is due to the fact that sources below 500 m are responsible for anomalies whose wavelengths are close to or larger than the size of the study area (~1 km wide).

6.3. Inversion of Magnetic Topography

In a third step, we assumed that magnetization direction and intensity are constant within the magnetic substratum (i.e., unaltered volcanic substratum) overlain by a nonmagnetic layer (i.e., altered or nonvolcanic substratum) of variable thickness and inverted magnetic anomalies for the topography of the magnetic substratum (Figure 10c). We follow a method developed by *Pilkington and Crossley* [1986] for the analysis of magnetic profiles, later applied for the joint inversion of gridded gravity and magnetic data [*Pilkington*, 2006]. In this study, this method is applied to ground and airborne magnetic data and used to evaluate the bottom of the hydrothermal alteration zone assuming hydrothermal alteration has completely demagnetized the volcanic substratum.

Within this method, *Pilkington and Crossley* [1986] suggested to iteratively modify the shape of the topography (z_i , z_{i+1} , etc) so its magnetic effect (ΔT_i , ΔT_{i+1} , etc) computed using the *Parker* [1972] method better fits the observed magnetic anomaly map. The correction at each step ($z_{i+1} - z_i$) is estimated from the discrepancies between the observed magnetic anomalies and the computed magnetic effect ($\Delta T_{\text{obs}} - \Delta T_i$) using Parker's formula (equation (2)) but only retaining the $n=1$ term:

$$z_{i+1} = z_i + \mathcal{T}^{-1} \left(\frac{\mathcal{T}(\Delta T_{\text{obs}} - \Delta T_i)}{-2\pi |\vec{k}| C_m M \theta_m \theta_b e^{-|\vec{k}| z_m} (1 - e^{-|\vec{k}| t})} \right) \quad (7)$$

Note that the method of *Pilkington and Crossley* [1986] was developed using matrix notations but is applied here in a more simple way applying the Fourier and inverse Fourier transformations. As equation (7) is not defined for $|\vec{k}| = 0$, we constrain the term in parenthesis of equation (7) to be equal to zero for $|\vec{k}| = 0$ before applying the inverse Fourier transform, which is equivalent to assuming that the averaged values of z_i and z_{i+1} are equal.

Iterations start from the real topography z_0 and are repeated until convergence (i.e., until the ratio of the norm of the increment $z_{i+1} - z_i$ to the norm of z_i is lower than 10^{-3}). This inversion tends to amplify the poorly constrained short-wavelength signal in the same way as the *Parker and Huestis* [1974] method does. For this reason, we apply, at each iteration, the low-pass filter defined in (4) to the topography correction with the following parameters: $k_h = 8 \times 10^{-3}$ rad/m (i.e., a wavelength ~790 m) and $k_h - w_h = 3 \times 10^{-3}$ rad/m (i.e., ~2100 m) for aeromagnetic data in areas 1–3, and $k_h = 5 \times 10^{-2}$ rad/m (i.e., ~130 m) and $k_h - w_h = 1 \times 10^{-2}$ rad/m (~630 m) for ground data in area 4. In order to avoid inversion results that yield solutions above the real topography, we replace, at each iterative step, the new magnetic topography $z_{i+1}(x, y)$ by the real topography $z_0(x, y)$ when $z_{i+1}(x, y) < z_0(x, y)$ ($z_i(x, y)$ is defined as the distance between the survey elevation and the topographic surface). The midvalue z_m of topography could be redefined at each step for the application of equation (7) but we decided not to do so to prevent the quantity $e^{-|\vec{k}| z_m}$ from becoming too small (numerically equal to zero) as z_m increases. The thickness of nonmagnetic substratum, assumed to correspond to the area of hydrothermal alteration, is simply obtained from $z_{i+1}(x, y) - z_0(x, y)$. The quality of the inversion is estimated by computing the root-mean-square (RMS) of the differences between the final magnetic effect ΔT_{i+1} and the observed magnetic anomaly map ΔT_{obs} . Note that, since we start our iterations from real topography z_0 and apply the low-pass filter only to the topography correction, the final topography z_{i+1} contains short wavelengths that are present in the real topography map but are not constrained by our inversion and should not be interpreted. However, these short wavelengths are removed when considering the thickness of the nonmagnetic substratum $z_{i+1}(x, y) - z_0(x, y)$.

Maps of the inverted topography and resulting thickness of nonmagnetic substratum in areas 1–4, obtained assuming a constant magnetization of 3 A/m or 5 A/m with a GAD field direction ($I = 63^\circ$, $D = 0^\circ$), are shown in the bottom row of Figures 12–15. Cross sections of the 3 A/m models are presented in Figure 16. Table 6

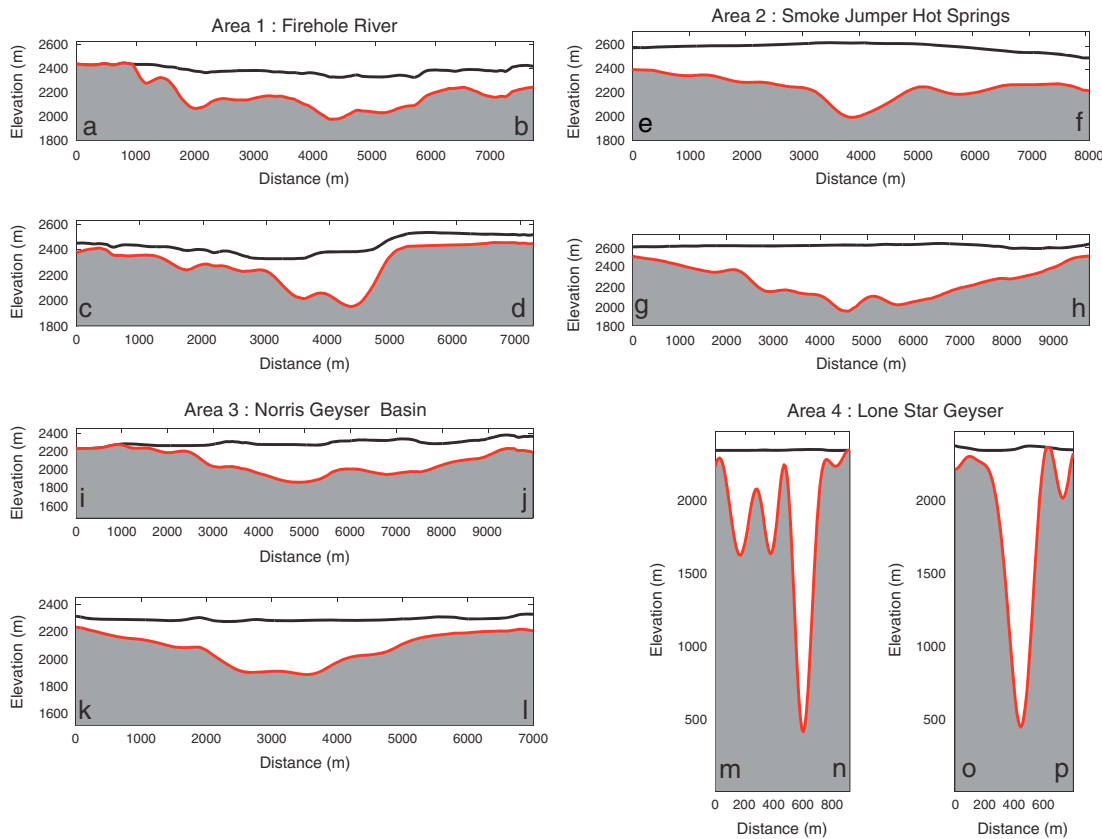


Figure 16. Cross sections of the thickness of nonmagnetic substratum in study areas 1–4 estimated assuming a constant magnetization of 3 A/m in the magnetic substratum: Firehole River, Smoke Jumper Hot Springs, Norris Geyser Basin, and Lone Star Geyser. Endpoints of cross sections are located on the bottom right plots of Figures 12–15. Magnetic and nonmagnetic substrata are represented in grey and white, respectively. Real topography and magnetic topography are represented by black and red lines, respectively.

shows that differences between observed anomalies and model predictions are very small for areas 1–4 (RMS of differences lower than 25 nT and ratio of RMS of differences over RMS of observed anomalies lower than 20%) although a bit larger than RMS obtained from the *Parker and Huestis* [1974] models. These slightly larger RMS values may have three explanations. First, the *Parker and Huestis* [1974] models include contrasts of magnetization intensity in the substratum beneath the ground surface and produce maps of magnetic anomalies containing smaller wavelengths compared to the *Pilkington and Crossley* [1986] models, which are composed of buried magnetic topography. Second, the low-pass filter was chosen here with slightly lower wave number cutoff points for the *Pilkington and Crossley* [1986] method to prevent unrealistic amplification of short-wavelength noise. Third, the Parker's formula is truncated to $n=1$ in equation (7) used for the *Pilkington and Crossley* [1986] models.

In the four areas, the deepest magnetic topography (i.e., the thickest nonmagnetic substratum) generally coincides with hydrothermal activity or alteration, as expected from the results of the *Parker and Huestis* [1974] inversion. Inversions performed assuming the lowest magnetization intensity (3 A/m) yield thicker but narrower volumes of nonmagnetic substratum that correlate very well with the location of surface hydrothermal features (see for instance areas 2 and 4 in Figures 13 and 15). The very deep extent (~2000 m) of the nonmagnetic feature obtained in area 4 assuming a magnetization intensity of 3 A/m seems in contradiction with the shallower extent (~500 m) of the nonmagnetic substratum obtained in area 1 assuming the same magnetization intensity. This may be explained first by the fact that the magnetic anomaly associated with the narrow feature obtained in area 4 is filtered out at the elevation of aeromagnetic data, or second by the fact that the magnetic low observed with the ground magnetic data over area 4 is likely due to the complete demagnetization of a strongly magnetized substratum (i.e., a contrast of magnetization intensity closer to 5 A/m

Table 6. Parameters and Results of the Magnetic Topography Inversion in Areas 1–4 Performed Using (7) and Assuming a GAD Field Direction: Magnetization Intensity of the Substratum Used for the Inversion, RMS of Differences Between Observed Magnetic Anomalies and Model Predictions, Relative RMS (i.e., Ratio of the RMS of Differences Over the RMS of Observed Anomalies), and Estimated Volume of Nonmagnetic Substratum Beneath the Investigated Area

Zone	M (A/m)	RMS (nT)	Relative RMS (%)	Volume (km ³)
Firehole River	3	6.7	5.9	11.4
	5	7.2	6.3	8.2
Smoke Jumper Hot Spring	3	17.0	17.8	19.8
	5	17.1	17.9	11.6
Norris Geyser Basin	3	9.5	14.7	18.7
	5	9.5	14.7	14.4
Lone Star Geyser	3	24.1	8.0	0.182
	5	18.2	6.0	0.058

between fresh and altered units), whereas the magnetic lows observed with aeromagnetic data are likely due to partial demagnetization or to a mélange of rock units with various degrees of demagnetization (i.e., leading to a contrast of magnetization intensity that is closer to 3 A/m between fresh and altered units).

Table 6 also displays the volume of nonmagnetic substratum deduced from the thickness maps of nonmagnetic substratum. As expected, assuming a lower value for magnetization intensity of fresh substratum yields larger volumes of nonmagnetic substratum. Beneath areas 1–3 (each covering a surface of ~100 km², see Figure 2), estimated volumes of nonmagnetic substratum range from ~10 to ~20 km³. Most of this nonmagnetic substratum is located beneath a small subregion of these areas.

Note that nonmagnetic substratum may include both initially nonmagnetic rocks and hydrothermally demagnetized rocks. Initially nonmagnetic rocks are observed in the central part of area 1 displaying alluvium at the contact between the three rhyolite flows (see Figure 2a) or in area 4 displaying a hill composed of hydrothermal deposits (see the topographic map on the top left corner of Figure 15). On the other hand, the nonmagnetic substratum in area 2 is most likely only composed of demagnetized substratum as this area includes a single rhyolite flow (see Figure 2b), and no hydrothermal deposits or alluvium are mapped at the surface.

The various models computed in this section assumed that the substratum hosts normal polarity magnetization. This is the case for the Lava Creek Tuff and the rhyolite flows that crop out in our study areas because they were formed during the last caldera cycle (after ~0.64 Ma). However, areas of hydrothermal alteration may also take place in deeper substrata (at depths of at least several hundred meters; see Christiansen [2001]) that were formed during older volcanic cycles and may host reverse polarity magnetizations. Because the depth and nature of these older substrata are not very precisely known, we did not take them into account in our models and this is therefore an additional source of uncertainty.

7. Discussion

In this section, we provide geological interpretations of our data analysis and inversions. Because of the nonuniqueness of potential field models, we must rely on simplifying assumptions in order to obtain single inverse models whose predictions best fit the observations. In fact, we produced two sets of models relying on two different sets of assumptions: magnetization of the substratum varying only in the horizontal direction (Figure 10b; inversion based on Parker and Huestis [1974]) versus constant magnetization in the volcanic substratum below a nonmagnetic layer (Figure 10c; inversion based on Pilkington and Crossley [1986]). Of course, our interpretations are dependent on the validity of our model assumptions, which include, for instance, that demagnetization associated with hydrothermal alteration reaches the surface. Our models are therefore not valid if a large volume of demagnetized rock is buried in the subsurface below a significant thickness of magnetic nonaltered substratum. In order to validate our assumptions, we would need to turn to other types of geophysical and geological data sets.

7.1. Origin of Magnetic Lows in Hydrothermal Sites

The first goal of our study was to understand the exact origin of magnetic lows observed in the high-resolution aeromagnetic survey of YNP over areas of hydrothermal activity (as described in Finn and Morgan

[2002]). In particular, we wanted to determine if they are due to partial or complete demagnetization of the volcanic substratum associated with hydrothermal alteration or to the presence of an initially nonmagnetic layer. Such distinction cannot be obtained from the analysis of aeromagnetic anomalies alone as magnetic lows can be almost equally well accounted for by a top layer of nonmagnetic or completely demagnetized substratum, as assumed in our *Pilkington and Crossley* [1986] inversions, or by horizontal variations of the degree of demagnetization, as assumed in our *Parker and Huestis* [1974] inversions. To answer this question, we would need to assess the average value and variability of magnetic susceptibility and remanence within fresh and altered geological units using a large number of nonweathered samples collected from various locations and depths in our study areas. As such large sampling is evidently not possible in hydrothermal areas of the YNP, we relied on ground magnetic surveys to constrain magnetic properties of superficial substratum and on rock samples from existing drill holes to constrain properties of deep substratum.

The damping of short-wavelength anomalies observed on ground magnetic transects over areas of hydrothermal activity and alteration indicates significant demagnetization of the shallow volcanic substratum associated with hydrothermal alteration. A similar relationship has been recognized from low-altitude aeromagnetic survey and used for epithermal deposit prospecting [e.g., *Irvine and Smith*, 1990]. We show here that such damping of short-wavelength anomalies can also be seen in ground magnetic profiles, used to map the demagnetization of the shallow substratum associated with hydrothermal alteration, and used to obtain a quantitative estimate of the depth to magnetic sources (i.e., the nonmagnetic terrain thickness). In this study, we use the gradient of magnetic anomalies measured along ground profiles to estimate an upper bound for depths to magnetic sources (Figure 9). Such depths are found to be greatest in areas displaying hydrothermal alteration with maximum values of the order of 100 m in area 2 (Smoke Jumper Hot Springs) to 1000 m in areas 1 (Firehole River) and 3 (Norris Geyser Basin).

However, the detailed ground survey acquired in area 4 (Lone Star Geyser) located within the area of damped anomalies of area 1 (Firehole River) shows prominent anomalies with amplitudes of several 100 nT and width of 50–100 m (see Figure 3), indicating that the volcanic substratum is not completely demagnetized but contains magnetic features at depths no greater than ~50–100 m. Such apparent contradiction with our estimated depth to sources (~1000 m in the regions of mapped hydrothermal alteration in areas 1 and 4) suggests in fact that demagnetization associated with hydrothermal areas is partial. Indeed, depth to sources estimated here are maximum depths obtained assuming a constant value for magnetization intensity contrasts that is relevant for fresh volcanic substratum. If the substratum has been partially demagnetized, it is likely to contain lower contrasts of magnetization intensity and therefore produce lower gradients of magnetic intensity. If total magnetization and magnetization intensity contrasts are divided by a factor of ~10 in hydrothermally altered units (as suggested by measurements performed on drill core samples), depths to sources estimated from the gradient of ground magnetic profiles also need to be divided by ~10 leading to maximum depths to sources of ~100 m in Lone Star Geyser consistent with the presence of 50–100 m wide anomalies in the detailed ground survey. Magnetic properties measured on drill core samples (Figure 6) also indicate that the degree of demagnetization varies rapidly with depth and lateral position (as evidenced by the differences observed between the nearby drill cores Y9 and Y12 in Norris Geyser Basin) indicating that demagnetization is heterogeneously distributed.

The magnetic low observed in the detailed ground magnetic survey in area 4 around the Lone Star Geyser and nearby hydrothermal features indicates more pervasive (possibly complete) demagnetization directly associated with the active vent. This is confirmed by results from the *Parker and Huestis* [1974] and the *Pilkington and Crossley* [1986] inversions which indicate a lower magnetization or a deeper extent of the demagnetized substratum centered on hydrothermal features. Such demagnetization is probably not a thermal demagnetization. Reservoir temperatures (i.e., maximum fluid temperatures) for liquid-dominated systems in YNP are estimated to be ~180–270°C and temperatures in shallow vapor-dominated systems range from ~150 to 240°C [e.g., *Fournier*, 1989]. These temperatures are much lower than the Curie temperature of magnetite or low-Ti titanomagnetite (i.e., ~560–580°C), the mineral that likely carries the stable magnetization in the unaltered substratum (as evidenced in the Lava Creek Tuff by *Reynolds* [1977]). Indeed, an elevation of the substratum temperature to ~200°C would only result in a decrease of the remanent magnetization of ~15% [see *Butler*, 1992, Figure 2.3]. The magnetic low observed in area 4 is therefore likely due to a larger degree of alteration. As a consequence, the altered volcanic substratum is probably best characterized by a heterogeneous magnetization that reflects rocks that have undergone

various degrees of partial demagnetization, with complete demagnetization limited to areas adjacent to faults or fractures through which the hydrothermal fluids circulate.

7.2. Geometry of Subsurface Hydrothermal Alteration

The second goal of our study was to provide constraints on the geometry of subsurface hydrothermal alteration, and in particular determine if alteration is distributed within a wide and shallow volume or instead within a narrow and deep rooted region. To this end, we produced two sets of models. The first set is obtained assuming magnetization is constant in the vertical direction in a layer of constant thickness or in a half-space below topography (*Parker and Huestis* [1974] inversion). These models amount to assuming demagnetization associated with hydrothermal alteration is localized in vertical pipes and are interpreted assuming the lowest magnetization occurs in the center of these hydrothermal pipes. In a second set of models, magnetization is constant in the three directions in a half-space beneath a layer of nonmagnetic substratum (*Pilkington and Crossley* [1986] inversion). These models are interpreted assuming that hydrothermal alteration has completely demagnetized the volcanic substratum and that this demagnetization is restricted to the shallow substratum. These two types of models both include parameters that are not well constrained, such as the magnetic layer thickness or the fresh (i.e., unaltered) substratum magnetization.

As already mentioned above, these two sets of models of magnetization account almost equally well for magnetic anomalies observed in the investigated areas. Nonetheless, we note that the narrow demagnetized structure, determined by a *Parker and Huestis* [1974] inversion assuming a half-space or by a *Pilkington and Crossley* [1986] inversion assuming low-magnetization intensity (3 A/m), generally coincides very well with surface hydrothermal activity and alteration. This coincidence cannot be fortuitous and suggests hydrothermal alteration is indeed located within narrow conduits beneath surface exposures of hydrothermal activity instead of spread out within wide and shallow areas (as is the case for instance in the 2-D models of *Finn and Morgan* [2002]). This conclusion may also be supported by the slightly smaller RMS of differences between observations and predictions obtained with the *Parker and Huestis* [1974] inversion that assumes vertical features (see Tables 5 and 6). Note, however, that these smaller RMS values may also simply be due to the use of low-pass filters with different wavelength cutoff or truncation of the Parker's formula at $n=1$ in the *Pilkington and Crossley* [1986] method. The large negative anomalies that extend beyond areas of hydrothermal alteration and activity may simply reflect large-wavelength anomalies produced by the deep part of the altered and nonmagnetic hydrothermal conduit. Such a distribution of hydrothermal alteration is consistent with a model where hydrothermal circulation and alteration are confined along fault and fracture zones.

Our study areas also display magnetic lows that do not correlate with surface exposure of hydrothermal alteration and cannot be attributed to geologic features or topographic effects. As examples, note the magnetic low located east of the hydrothermal site of Smoke Jumper Hot Springs in area 2 and the magnetic low northeast of the hydrothermal site of Norris Geyser Basin in area 3. These anomalies are not associated with damping of ground short-wavelength magnetic anomalies (except in a short part of the ground profile acquired at the edge of the magnetic low observed in area 3) indicating that the shallow substratum is not demagnetized (see Figure 7). These anomalies may therefore result from hydrothermal activity and alteration that has not reached the surface.

7.3. Comparisons Between Different Study Areas

The investigated areas 1–3 are characterized by different types of substratum (rhyolite flow versus tuff), geography (valley versus plateau), geologic context (outside, inside, or along the rim of the caldera), hydrothermal activity (liquid- versus vapor-dominated system), and chemistry of hydrothermal fluids (neutral to acidic waters with various contents in Cl^- , SiO_2 , and SO_4^{2-}). Nonetheless, these areas all display a damped short-wavelength signal in ground magnetic profiles and a large negative anomaly in the aeromagnetic survey indicating demagnetization of the volcanic substratum is present both at the surface and at depth. Therefore, these areas all underwent a past or recent episode of hydrothermal alteration that significantly decreased or destroyed the volcanic substratum magnetization. Assuming a magnetization intensity of ~3 A/m, we obtain in areas 1–3 a maximum thickness of nonmagnetic substratum of ~300–700 m.

As mentioned before, not all episodes of hydrothermal alteration are expected to demagnetize the substratum. Indeed, *Hochstein and Soengkono* [1997] suggested that alteration of titanomagnetite is expected in the case of liquid-dominated systems, as the environment is generally reducing (magnetite

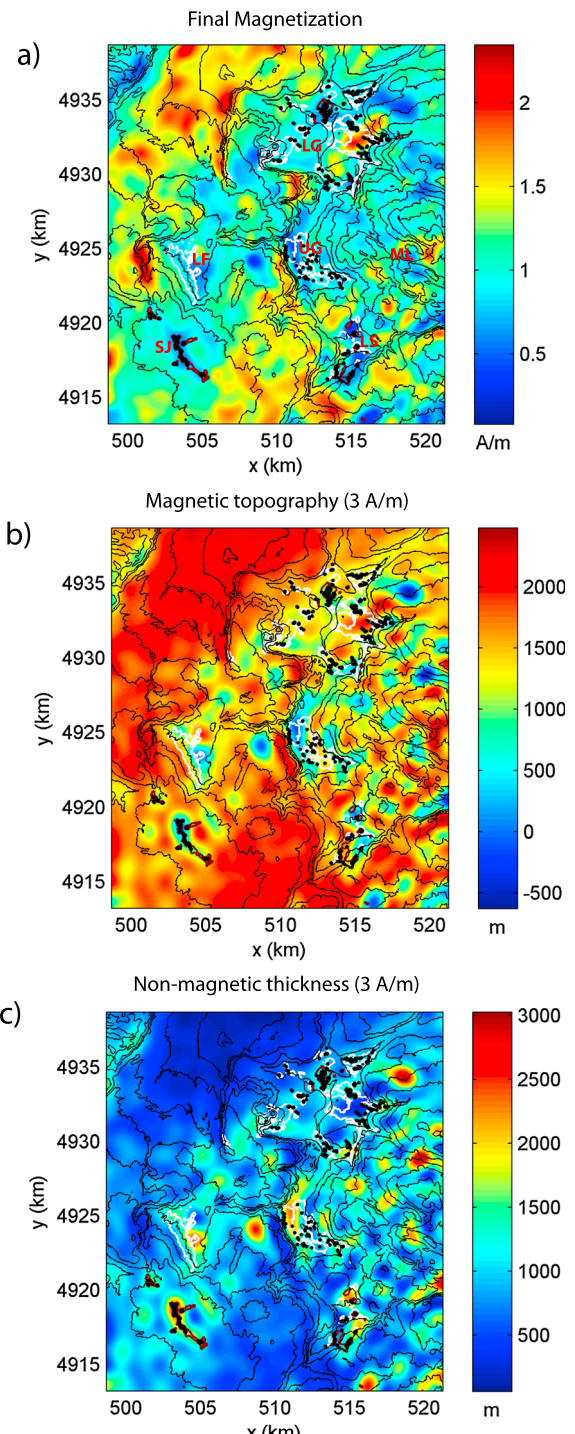


Figure 17

alteration (see profile in Figure 2b), suggesting that the location of the location of the demagnetized zones are not necessarily associated with the current episode of hydrothermal activity.

The inferred lateral extents of altered substratum are different in areas 1–3 (see zones of maximum nonmagnetic thickness on the bottom right plot of Figures 12–15). In area 1, altered substratum is located in the proximity of the valley but does not follow exactly its trend. It has instead a rather complicated path that

replaced by sulfides such as pyrite), but not necessarily in the deep part of vapor-dominated systems as the environment is generally oxidizing. Demagnetization is nonetheless observed both in the shallow and deep substratum of area 2 (Smoke Jumper Hot Springs), which is a vapor-dominated system. Demagnetization in the shallow substratum could be due to a recent episode of hydrothermal alteration as acidic condensates produced at the top part of the vapor-dominated system may alter magnetite (the solubility of magnetite increases with decreasing pH), whereas demagnetization in the deep substratum could be due to a past episode of hydrothermal alteration when the site was a liquid-dominated system, as proposed by Hochstein and Soengono [1997]. Indeed, the Smoke Jumper Hot Springs area was probably a liquid-dominated system during the last glaciation when the water table was higher since such a change from a liquid-to-a vapor-dominated system has been evidenced in drill core Y11 [Bargar and Muffler, 1982] located in the Mud Volcano vapor-dominated system. However, the damping of short-wavelength anomalies observed in area 2 is not as pronounced as in areas 1 and 3 and is restricted to a much narrower zone. Moreover, the depths to the top of magnetic sources (Figure 9) are much smaller in area 2 (<100 m) than in areas 1 and 3 (> 500 m), suggesting that alteration may be discontinuous with depth in the vapor-dominated system of area 2 (shallow alteration associated with acidic condensates versus deep alteration associated with the hydrothermal reservoir) but continuous in the liquid-dominated systems of areas 1 and 3. Finally, the area of damped anomalies in area 2 does not always coincide with the location of surface

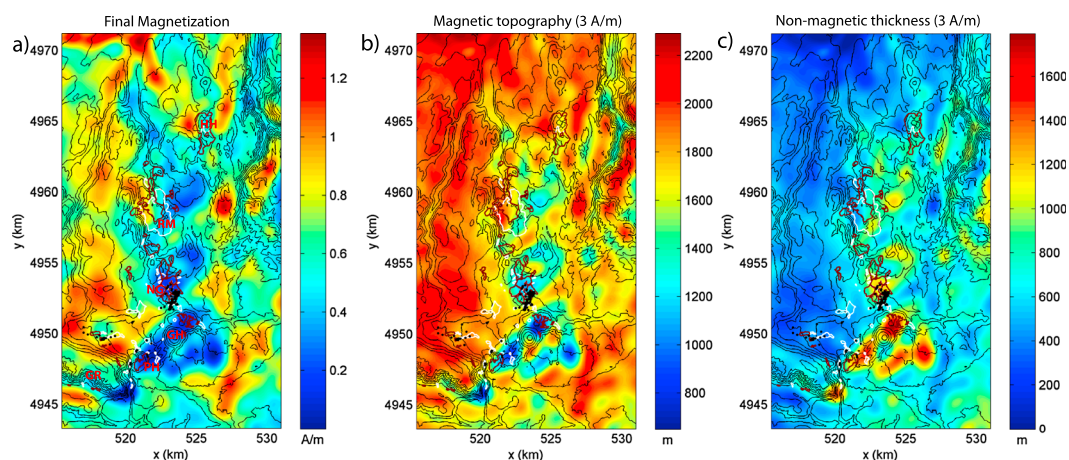


Figure 18. Same legend as in Figure 17 but for area e located by a green rectangle in Figure 1. Letter codes in Figure 18a show locations of places or features: GH, Gibbon Hill; GR, Gibbon River; HH, Horseshoe Hill; NG, Norris Geyser Basin; PH, Paintpot Hill; and RM, Roaring Mountain.

possibly reflects the location of contacts between rhyolite flows where fluid circulation is likely easier. In area 2, the location of altered substratum is linear and follows the direction of the nearby caldera rim probably because fractures associated with the caldera facilitate fluid circulation. In area 3, altered substratum covers a wide zone. This area is composed of rather impermeable tuffs but is also affected by many faults or fractures that likely facilitate fluid circulation.

7.4. Extension to Wider Areas

Finally, we performed inversions on larger areas including several hydrothermal sites: areas d and e (see green rectangles in Figure 1 and Figures 17, 18). The purpose of these inversions was first to compare nearby hydrothermal sites in terms of degree of demagnetization, depth to bottom, and thickness of demagnetized (i.e., altered) substratum; and second to possibly detect hidden buried volumes of altered substratum. Because these areas include larger topographic elevation changes than the small areas 1–3, the average distance between topography and upward continued aeromagnetic map is also higher. For these large areas, we therefore used different parameters for the low-pass filters: $k_h = 7 \times 10^{-3}$ rad/m (i.e., a wavelength of ~ 900 m) and $k_h - w_h = 2 \times 10^{-3}$ rad/m (i.e., ~ 3100 m) for areas d versus $k_h = 6 \times 10^{-3}$ rad/m (i.e., ~ 1000 m) and $k_h - w_h = 1 \times 10^{-3}$ (i.e., ~ 6300 m) for area e for the Parker and Huestis [1974] inversion and $k_h = 4 \times 10^{-3}$ rad/m (i.e., ~ 1600 m) and $k_h - w_h = 2 \times 10^{-3}$ rad/m (i.e., ~ 3100 m) for both areas for the Pilkington and Crossley [1986] inversion.

As mentioned earlier, the distribution of magnetization consistent with the Parker and Huestis [1974] assumptions and with the aeromagnetic data is nonunique. To overcome this problem, we assumed that the minimum value of magnetization observed within our study area was 0 A/m (i.e., the substratum has been completely demagnetized by alteration in parts of the study area). The same ambiguity exists for the magnetic topography consistent with the Pilkington and Crossley [1986] assumptions and with the aeromagnetic data. Our procedure yields a topography that coincides with the real topography within the study area. This was done by using the real topography as the initial model and forcing the topography of the magnetic substratum at each iteration to be below or equal to the real topography. We use the same procedures and assumptions for inversions on larger areas. However, because the conditions of a minimum value of magnetization or the coincidence of magnetic and real topographies are imposed on wider areas,

Figure 17. (a) Magnetization, (b) topography of magnetic substratum, and (c) thickness of nonmagnetic substratum in area d located by a green rectangle in Figure 1. These maps are obtained assuming magnetization is either constant in the vertical direction (Figure 17a) or constant in the three directions and equal to 3 A/m (Figures 17b and 17c) in a half-space below topography. Black lines are topographic contours represented with a 50 m spacing. Magnetization is assumed to have a GAD field direction. Letter codes in Figure 17a show locations of places or features: LG, Lower Geyser Basin; LF, Little Firehole Meadow; LS, Lone Star Geyser; ML, Mallard Lake Resurgent Dome; SJ, Smoke Jumper Hot Springs; and UG, Upper Geyser Basin.

we do not expect to obtain results that agree with those determined for the small areas 1–3. Instead, we expect to obtain larger values of magnetization, deeper magnetic topography and thicker nonmagnetic substratum for the larger area. Indeed, because the degree of demagnetization may vary from one hydrothermal area to another, imposing the condition of a minimum value of 0 A/m for magnetization intensity to the wider study areas would lead to an inverted map of magnetization intensity that display a value of 0 A/m in only the few areas characterized by the largest degrees of demagnetization and alteration. In the same way, because the base of the demagnetized layer may be more or less deep in the various hydrothermal sites and may not in some areas reach the ground surface, the coincidence of magnetic topography and real topography will only be observed in the few areas characterized by the largest substratum magnetization at the ground surface. Slightly larger values are indeed obtained for magnetization (compare Figure 17a with Figures 12 and 13, and Figure 18a with Figure 14) and much larger values are obtained for depth and thickness of nonmagnetic substratum in these larger areas. Note, however, that the assumption of constant magnetization (especially in the horizontal direction) may not be relevant for large areas such as areas d and e that include different geologic units (e.g., rhyolite and basalt flows or ash flow tuffs) likely to be characterized by different magnetic properties.

The map of magnetization in area d (Figure 17a) shows that its major hydrothermal sites (i.e., Smoke Jumper Hot Springs, SJ, in area 2; Lone Star Geyser, LS, in areas 1 and 4; Upper Geyser Basin, UG; Lower Geyser Basins, LG; and Little Firehole Meadows, LF) are all characterized by a significantly decreased magnetization (almost 0 A/m). Several areas that do not display hydrothermal activity or alteration at the surface are also characterized by very low magnetization, for instance in the Mallard Lake Resurgent Dome (ML). This could be due either to different initial magnetic properties of the Mallard Lake rhyolite flow constituting the dome (with respect to the other nearby rhyolite flows) or to some early or buried hydrothermal alteration which would have been facilitated by the large density of faults observed in the resurgent dome. Assuming the fresh volcanic substratum bears a relatively constant magnetization, the map of the magnetic substratum elevation (Figure 17b) seems to indicate that its lowest point is located around Upper Geyser Basin (UG) and that the maximum thickness of demagnetized substratum (Figure 17c) is located beneath Smoke Jumper Hot Spring (SJ). On the other hand, these maps show that some areas are devoid of alteration (see in the northeast and southeast of area d).

The map of magnetization in area e (Figure 18a) shows three main patches of low magnetization. These patches include the major hydrothermal sites in area e (i.e., Norris Geyser Basin, NG, in area 3; Paintpot Hill, PH; Roaring Mountain, RM) but they also include large areas with no surface alteration or activity. These patches may be due either to large volumes of buried alteration or to changes in the lithology. The northeast patch is indeed coincident with the location of Obsidian Cliff flow and the southeast patch is coincident with the location of the Gibbon River flow. On the other hand, the Norris Geyser Basin patch is not associated with any change in the lithology. Therefore, the part of this anomaly that does not correlate with mapped hydrothermal alteration may indicate concealed hydrothermal activity and alteration that did not reach the surface.

8. Conclusions

Magnetic lows observed in the aeromagnetic survey and damped short-wavelength signal observed in ground magnetic profiles over areas of hydrothermal activity and alteration indicate that demagnetization occurs in the shallow and deep substratum within all the investigated areas, including both liquid- and vapor-dominated systems. Degrees of demagnetization may vary within the area of hydrothermal alteration and reach complete demagnetization within the hydrothermal plumbing system, as suggested by the occurrence of a pronounced magnetic low centered on the Lone Star Geyser. Measurements on rock samples show that a significant decrease of the substratum total magnetization is observed within altered zones but that the degree of demagnetization varies dramatically over short distance.

The amplitude of short-wavelength anomalies can be used to map areas of hydrothermal alteration by searching areas characterized by amplitudes lower than a threshold. This threshold depends on geologic units and can, for instance, be chosen to be half the amplitudes of short-wavelength anomalies observed over the unaltered unit. The lower gradients observed over magnetic profiles in areas of hydrothermal alteration indicate deeper sources as shown by the application of the *Smith* [1959] method (if alteration yields complete

demagnetization) or lower contrasts of magnetization intensity within the volcanic substratum (if alteration yields partial demagnetization). The even lower amplitude and gradient of magnetic anomalies observed around the location of the Lone Star Geyser confirm that the vent area is characterized by a more complete alteration.

Only a few areas within or nearby the Yellowstone caldera display magnetic anomalies that agree with magnetic anomalies calculated from topography assuming constant magnetization. This indicates that most areas are not characterized by a constant magnetization. In addition, we found that magnetic lows observed over areas of hydrothermal alteration cannot be attributed to topography. Inversion of the substratum magnetization using the *Parker and Huestis* [1974] method shows that maximum degree of demagnetization coincides with the location of hydrothermal activity and alteration. Assuming a deeper extent of demagnetization yields smaller contrasts of magnetization intensity between altered and unaltered substratum and narrower zones of demagnetization that even better coincide with hydrothermal features. Inversion of the topography of the magnetic (i.e., unaltered) substratum using the *Pilkington and Crossley* [1986] method shows that the deepest magnetic substratum (i.e., thickest nonmagnetic substratum) generally coincides with the location of hydrothermal activity and alteration. Assuming a smaller magnetization intensity for the unaltered substratum yields deeper and narrower zones of demagnetization that also better coincide with hydrothermal features. Assuming magnetization of the unaltered volcanic substratum is 3 A/m yields thicknesses and volumes of nonmagnetic substratum of ~300–700 m and ~10–20 km³, respectively.

From the above results, we conclude that the sources of magnetic lows observed over areas of mapped hydrothermal alteration are rocks that have undergone various degrees of partial demagnetization due to alteration, with a larger degree or complete demagnetization within the hydrothermal plumbing system. Although our inversions are nonunique, we conclude that demagnetization (and hydrothermal alteration) most likely corresponds to narrow and deep features rather than shallow and wide features. Although both deep and shallow demagnetization are observed, ground magnetic profiles over the vapor-dominated system of area 2 (Smoke Jumper Hot Springs) suggest smaller degrees of demagnetization in the shallow substratum or discontinuous demagnetization with depth (shallow alteration associated with acidic condensates versus deep alteration associated with the hydrothermal reservoir) in comparison with the liquid-dominated systems of areas 1 and 3 that would be characterized by more continuous demagnetization (from shallow to deep substratum). Extension of these inversions to larger areas allows us to compare distinct hydrothermal areas in terms of degree of alteration, depth of the bottom of the altered zone, or thickness of altered substratum.

Acknowledgments

We are grateful to Jake Lowenstern, Shaul Hurwitz, and Patrick Muffler for helpful discussions and suggestions and to Darcy K. McPhee, Barbara Sue Jessup, Sandra Jean Underwood, Nellie Olsen, Erin Looby, and Claire Pontbriand for their participation in the field data collection. Thorough reviews by Mark J. Dekkers, Fabio Caratori Tontini, and an anonymous reviewer helped to clarify and improve the paper. Airborne magnetic data used in this study are available online at <http://pubs.usgs.gov/of/2000/ofr-00-0163/>. Ground magnetic data are not published but are available from the first author upon request. This research was funded by the U.S. Geological Survey's Geothermal Resource Investigations Project. Part of this work was supported by a Lavoisier grant from the French Ministry of Foreign Affairs (to C. Bouligand). ISTerre is part of OSUG@2020 (ANR10 LABX56).

References

- Bargar, K. E., and M. H. Beeson (1984), Hydrothermal alteration in research drill hole Y-6, Upper Firehole River, Yellowstone National Park, *U.S. Geol. Surv. Prof. Pap.* 1054-B.
- Bargar, K. E., and L. J. P. Muffler (1982), Hydrothermal alteration in research drill hole Y-11 from a vapor-dominated geothermal system at Mud Volcano, Yellowstone National Park, Wyoming, Thirty-Third Annual Field Conference, Wyoming Geological Association Guidebook.
- Blakely, R. J. (1995), *Potential Theory in Gravity and Magnetic Applications*, Cambridge Univ. Press, Cambridge, U. K.
- Blakely, R. J., and R. L. Christiansen (1978), The magnetization of Mount Shasta and implications for virtual geomagnetic poles determined from seamounts, *J. Geophys. Res.*, 83, 5971–5978, doi:10.1029/JB083B12p05971.
- Bott, M. H. P., and R. A. Smith (1958), The estimation of the limiting depth of gravitating bodies, *Geophys. Prospect.*, 6, 1–10.
- Bouligand, C., J. M. G. Glen, and R. J. Blakely (2009), Mapping Curie temperature depth in the western United States with a fractal model for crustal magnetization, *J. Geophys. Res.*, 114, B11104, doi:10.1029/2009JB006494.
- Butler, R. F. (1992), *Paleomagnetism: Magnetic Domains to Geologic Terranes*, pp. 237, Blackwell Scientific Publications, Oxford, U. K.
- Christiansen, R. L. (2001), The Quaternary and Pliocene Yellowstone Plateau volcanic field of Wyoming, Idaho, and Montana, *U.S. Geol. Surv. Prof. Pap.* 729-G.
- Christiansen, R. L. (1975), Geological map of the Norris Junction quadrangle, Yellowstone National Park, Wyoming, U.S. Geological Survey Geologic Quadrangle 1193.
- Christiansen, R. L., and H. R. Blank (1974), Geological map of the Old Faithful quadrangle, Yellowstone National Park, Wyoming, U.S. Geological Survey Geologic Quadrangle 1189.
- Christiansen, R. L., and R. R. Wahl (1999), Digital geologic map of Yellowstone National Park, Idaho, Montana, and Wyoming and vicinity, *U.S. Geol. Surv. Open File Rep.*, 99-0174. [Available at <http://greenwood.cr.usgs.gov/pub/open-file-reports/ofr-99-0174/>.]
- Cordell, L. (1985), Techniques, applications, and problems of analytical continuation of New Mexico aeromagnetic data between arbitrary surfaces of very high relief, in *Proceedings of the International Meeting on Potential Fields in Rugged Topography*, Bulletin No. 7, pp. 96–99, Institute of Geophysics, University of Lausanne, Switzerland.
- Fedi, M., and G. Florio (2013), Determination of the maximum-depth to potential field sources with a maximum structural index method, *J. Appl. Geophys.*, 88, 154–160.
- Finlay, C. C., et al. (2010), International Geomagnetic Reference Field: The eleventh generation, *Geophys. J. Int.*, 183, 1216–1230.

- Finn, C. A., and L. A. Morgan (2002), High-resolution aeromagnetic mapping of volcanic terrain, Yellowstone National Park, *J. Volcanol. Geotherm. Res.*, 115, 207–231.
- Fournier, R. O. (1989), Geochemistry and dynamics of the Yellowstone National Park hydrothermal system, *Annu. Rev. Earth Planet. Sci.*, 17, 13–53.
- Francheteau, J., C. G. A. Harrison, J. G. Sclater, and M. L. Richards (1970), Magnetization of Pacific Seamounts: A preliminary polar curve for the northeastern Pacific, *J. Geophys. Res.*, 75, 2035–2061, doi:10.1029/JB075i011p02035.
- Harlan, S. S., and L. A. Morgan (2008), Paleomagnetism and rock magnetic properties from quaternary lavas and tuffs of the Yellowstone Plateau Volcanic Field, AGU Fall Meeting, Abstract GP11A-0686.
- Hellman, M. J., and M. S. Ramsey (2004), Analysis of hot springs and associated deposits in Yellowstone National Park using ASTER and AVIRIS remote sensing, *J. Volcanol. Geotherm. Res.*, 135, 195–219.
- Hochstein, M. P., and S. Soengkono (1997), Magnetic anomalies associated with high temperature reservoirs in the Taupo Volcanic Zone (New Zealand), *Geothermics*, 26, 1–24.
- Hunt, C. P., B. M. Moskowitz, and S. K. Banerjee (1995), Magnetic properties of rocks and minerals, in *Rock Physics and Phase Relations: A Handbook of Physical Constants*, edited by T. J. Ahrens, pp. 189–204, AGU, Washington, D. C.
- Irvine, R. J., and M. J. Smith (1990), Geophysical exploration for epithermal gold deposits, *J. Geochem. Explor.*, 36, 375–412.
- Lecoanet, H., F. Leveque, and S. Segura (1999), Magnetic susceptibility in environmental applications: Comparison of field probes, *Phys Earth Planet. Int.*, 115, 191–204.
- Lowenstern, J. B., D. Bergfeld, W. C. Evans, and S. Hurwitz (2012), Generation and evolution of hydrothermal fluids at Yellowstone: Insights from the Heart Lake Geyser Basin, *Geochem. Geophys. Geosyst.*, 13, Q01017, doi:10.1029/2011GC003835.
- Livo, K. E., F. A. Kruse, R. N. Clark, R. F. Kokaly, and W. C. Shanks III (2007), Hydrothermally altered rock and hot-spring deposits at Yellowstone National Park characterized using airborne visible- and infrared-spectroscopy data, in *Integrated Geoscience Studies in the Greater Yellowstone Area—Volcanic, Tectonic, and Hydrothermal Processes in the Yellowstone Geosystem*, U.S. Geol. Surv. Prof. Pap. 1717, edited by L. A. Morgan, pp. 493–505.
- National Park Service (2007), Digital geological map of Yellowstone National Park and vicinity, Wyoming, Montana and Idaho, NPS Geologic Resources Inventory Program, Geospatial Dataset-1044842.
- Nettleton, L. L. (1939), Determination of density for reduction of gravimeter observations, *Geophysics*, 4, 176–183.
- Oliver, H. W., and R. L. Christiansen (1998), Locations, descriptions, densities, and magnetic susceptibilities of rock samples collected for analyses of gravity and aeromagnetic anomalies in Yellowstone National Park, Wyoming, Idaho, and Montana, *U.S. Geol. Surv. Open File Rep.*, 98–247.
- Parker, R. L. (1972), The rapid calculation of potential anomalies, *Geophys. J. R. Astron. Soc.*, 31, 447–455.
- Parker, R. L., and S. P. Huestis (1974), Inversion of magnetic anomalies in the presence of topography, *J. Geophys. Res.*, 79, 1587–1593.
- Percival, D. B., and A. T. Walden (1993), *Spectral Analysis for Physical Applications: Multitaper and Conventional Univariate Techniques*, Cambridge Univ. Press, New York.
- Peters, L. (1949), The direct approach to magnetic interpretation and its practical application, *Geophysics*, 14, 290–320, doi:10.1190/1.1437537.
- Pilkington, M. (2006), Joint inversion of gravity and magnetic data for two-layer models, *Geophysics*, 71, L35–L42, doi:10.1190/1.2194514.
- Pilkington, M., and D. J. Crossley (1986), Determination of crustal interface topography from potential fields, *Geophysics*, 51, 1277–1284.
- Reid, A. B., J. M. Allsop, H. Granser, A. J. Millott, and I. W. Somerton (1990), Magnetic interpretation in three dimensions using Euler deconvolution, *Geophysics*, 55, 80–91.
- Reynolds, L. R. (1977), Paleomagnetism of welded tuffs of the Yellowstone Group, *J. Geophys. Res.*, 82, 3677–3693.
- Roest, W. R., J. Verhoef, and M. Pilkington (1992), Magnetic interpretation using the 3D analytic signal, *Geophysics*, 57, 116–125.
- Schouten, H., and K. McCamy (1972), Filtering marine magnetic anomalies, *J. Geophys. Res.*, 77, 7089–7099.
- Smith, R. A. (1959), Some depth formulae for local magnetic and gravity anomalies, *Geophys. Prospect.*, 7, 55–63.
- Talwani, M. (1965), Computation with the help of a digital computer of magnetic anomalies caused by bodies of arbitrary shape, *Geophysics*, 30, 797–817, doi:10.1190/1.1439654.
- Thompson, D. T. (1982), EULDPH: A new technique for making computer-assisted depth estimates from magnetic data, *Geophysics*, 47, 31–37.
- U. S. Geological Survey (2000), An aeromagnetic survey in Yellowstone National Park: A web site for distribution of data (on-line edition), *USGS Open File Rep. 00-163*. [Available at <http://pubs.usgs.gov/of/2000/ofr-00-0163/>.]
- Werner, S. (1953), Interpretation of magnetic anomalies at sheet-like bodies, *Sveriges Geol. Undersok.*, Arsbok, 43, no. 6, series C, no 508.
- White, D. E. (1957), Thermal waters of volcanic origin, *Geol. Soc. Am. Bull.*, 68, 1637–1658.
- White, D. E., L. J. P. Muffler, and A. H. Truesdell (1971), Vapor-dominated hydrothermal systems compared with hot-water systems, *Econ. Geol.*, 66, 75–97.
- White, D. E., R. O. Fournier, L. J. P. Muffler, and A. H. Truesdell (1975), Physical results of research drilling in thermal areas of Yellowstone National Park, Wyoming, *U.S. Geol. Surv. Prof. Pap.* 892.
- White, D. E., R. A. Hutchinson, and T. E. C. Keith (1988), The geology and remarkable thermal activity of Norris Geyser basin, Yellowstone National Park, Wyoming, *USGS Prof. Pap.* 1456.